

Mass spectrum of the minimal SUSY $B - L$ model

Ben O’Leary^{1,a}, Werner Porod^{1,b}, Florian Staub^{1,2,c}

¹*Institut für Theoretische Physik und Astrophysik, Universität Würzburg,
97074 Würzburg, Germany*

²*Physikalisches Institut der Universität Bonn,
53115 Bonn, Germany*

^a*Email: ben.oleary@physik.uni-wuerzburg.de*

^b*Email: porod@physik.uni-wuerzburg.de*

^c*Email: fnstaub@th.physik.uni-bonn.de*

ABSTRACT: The origin of R -parity in supersymmetric models can be explained if $B - L$ is part of the gauge group. We discuss the mass spectrum of the minimal $U(1)_Y \times U(1)_{B-L}$ model based on a GUT implementation using CMSSM-like boundary conditions. Here we focus in particular on the Higgs and neutralino sectors in this class of models. While the neutralinos can have masses as low as 100 GeV, we show that the requirement of being consistent with existing bounds on the Z' implies that in general the sfermions have masses in the multi-TeV range. In the extended Higgs sector we show the existence of a second light state which, however, will be difficult to observe, while having at the same time a SM-like Higgs in a mass range of 123-126 GeV. Moreover, we propose a set of benchmark scenarios for phenomenological studies. On the technical side we demonstrate that gauge kinetic mixing effects can be quite important, affecting in particular the Higgs and the neutralino sectors. Not only can they shift the mass of the lightest neutralino by about 10 per-cent but also they can change the nature of neutralinos and Higgs bosons in a significant way.

Contents

1. Introduction	1
2. The Model	3
2.1 Particle content and superpotential	3
2.2 Gauge kinetic mixing	4
2.3 Tadpole equations	6
2.4 Gauge boson mixing	8
2.5 The Higgs sector	10
2.5.1 Pseudoscalar Higgs bosons	10
2.5.2 Scalar Higgs bosons	10
2.5.3 The charged Higgs boson	11
2.6 Neutralinos	11
2.7 Charginos and sfermions	13
2.8 Boundary conditions at the GUT scale	14
3. Numerical results	15
3.1 Benchmark Points	16
3.2 Precision of the mass calculation: the impact of kinetic mixing	17
3.3 The Higgs sector	19
3.4 The neutralino sector	24
4. Conclusions and discussion	28
A. Mass matrices	28
B. RGEs	29
B.1 Anomalous dimensions	30
B.2 Gauge Couplings	31
B.3 Gaugino Mass Parameters	31
C. Model files for SARAH	32
C.1 B-L-SSM.m	32
C.2 SPheno.m	34

1. Introduction

Models with an additional $U(1)_{B-L}$ gauge symmetry at the TeV scale have recently received considerable attention. On one hand, they are among the simplest extensions of Standard Model (SM) gauge group with observable consequences at the LHC [1, 2, 3, 4]. On the other, this class of models can help to understand the origin of

R -parity and its possible spontaneous violation in supersymmetric models [5, 6, 7], as well as the mechanism of leptogenesis [8, 9]. It has been shown that a gauge sector containing $U(1)_Y \times U(1)_{B-L}$ can be a result of an $E_8 \times E_8$ heterotic string theory (and hence M-theory) [10]. While most studies of supersymmetric variants have so far focused on the effects of the additional gauge group far below the GUT scale, the questions arise of whether this group can be unified at the high scale with the SM gauge group and what the phenomenological consequences are. A renormalization group equation (RGE) analysis of such a model, assuming the unification of the gauge groups, has been performed in [7, 11]. However, the effects of possible mixing between the two Abelian groups have been neglected so far: it is well known that in models with several $U(1)$ gauge groups, kinetic mixing terms

$$-\chi_{ab} \hat{F}^{a,\mu\nu} \hat{F}_{\mu\nu}^b, \quad a \neq b \quad (1.1)$$

between the field strength tensors are allowed by gauge and Lorentz invariance [12], as $\hat{F}^{a,\mu\nu}$ and $\hat{F}^{b,\mu\nu}$ are gauge invariant quantities by themselves, see *e.g.* [13]. Even if these terms are absent at tree level at a particular scale, they might be generated by RGE effects [14, 15].

The impact of gauge kinetic mixing in generic extensions of the standard model (SM) and the MSSM has been studied so far in several aspects. For instance, one can show that the dark matter of the universe can be charged with respect to an additional $U(1)$ but neutral with respect to the SM gauge group. However, here one can show that there is a residual SM gauge interaction of the dark matter particles due to the gauge kinetic mixing. The consequences for the relic density and the cross sections concerning direct as well indirect detection of dark matter have been analyzed [16, 17, 18]. It has been shown that these cosmological bounds are sometimes more severe than the bounds from electroweak precision data if the dark matter candidate interacts dominantly due to kinetic mixing. Moreover, the kinetic mixing in the context of supersymmetric hidden sector dark matter has been considered in [19] and the LHC phenomenology of a nearly decoupled sector only interacting with the visible sector due to kinetic mixing has been elaborated in [20].

In this work, we discuss the mass spectrum of the model presented in [5, 7]. This minimal $B - L$ extension of the Minimal Supersymmetric Standard Model (MSSM) has a $U(1)_{B-L}$ gauge group tensored to the SM gauge groups and two bileptonic chiral superfields which are gauge singlets under SM gauge groups. In addition, three right-handed neutrinos are needed to ensure that $U(1)_{B-L}$ is anomaly-free, which provide the necessary ingredients to explain neutrino data. We refer to this model as the BLSSM.

The focus of this paper is on the mass spectrum of this model and resulting phenomenological aspects assuming mSUGRA-like boundary conditions at the GUT scale and unification of the $B - L$ coupling with the SM couplings. In particular we will demonstrate that gauge kinetic mixing effects are particularly important in the

Higgs and neutralino sectors. These effects do not only change the masses of these particles but have quite some impact on their nature, *e.g.* they induce tree-level mixing which would be absent if these effects were to be neglected. We will show that new light Higgs states are possible without being in conflict with current data while having at the same time a SM-like Higgs in the range close to 120 GeV. We will focus here on the case of R-parity conservation and discuss the case of broken R-parity violation in a subsequent paper [21].

In the usual CMSSM with the MSSM particle content, the lightest neutralino is mainly bino-like. We show that in our model the nature of this particle can be quite different and identify regions where it is either mainly a $SU(2)_L$ -doublet Higgsino, a $U(1)_{B-L}$ -gaugino which we dub the BLino, or a fermionic partner of the $U(1)_{B-L}$ -breaking scalar which we dub the bileptino, since we call the scalar the bilepton for reasons given below. In the next section we introduce the model and focus in particular on aspects related to the spectrum. In section 3 we present our numerical results and provide benchmark points with distinct features and in section 4 we draw our conclusions. In the appendices we collect supplementary formulas for mass matrices, anomalous dimensions and β -functions at lowest order needed for the discussion of the main features in section. The corresponding formulas including higher order effects can be easily computed using the input files for SARAH given in appendix C.

2. The Model

In this section we present the particle content of the model considered. An important aspect is the $U(1)$ gauge kinetic mixing which is discussed in some detail as it leads to significant changes in the spectrum. Although we include loop corrections for the numerical analysis when calculating the masses, we restrict ourselves in this section to tree-level expressions, as this is sufficient for discussing the main differences with respect to the MSSM.

2.1 Particle content and superpotential

The model consists of three generations of matter particles including right-handed neutrinos which can, for example, be embedded in $SO(10)$ 16-plets. Moreover, below the GUT scale the usual MSSM Higgs doublets are present as well as two fields η and $\bar{\eta}$ responsible for the breaking of the $U(1)_{B-L}$. Furthermore, η is responsible for generating a Majorana mass term for the right-handed neutrinos and thus we interpret the $B - L$ charge of this field as its lepton number, and likewise for $\bar{\eta}$, and call these fields bileptons since they carry twice the lepton number of (anti-)neutrinos. We summarize the quantum numbers of the chiral superfields with respect to $U(1)_Y \times SU(2)_L \times SU(3)_C \times U(1)_{B-L}$ in Table 1.

Superfield	Spin 0	Spin $\frac{1}{2}$	Generations	$(U(1)_Y \otimes SU(2)_L \otimes SU(3)_C \otimes U(1)_{B-L})$
\hat{Q}	\tilde{Q}	Q	3	$(\frac{1}{6}, \mathbf{2}, \mathbf{3}, \frac{1}{6})$
\hat{D}	\tilde{d}^c	d^c	3	$(\frac{1}{3}, \mathbf{1}, \bar{\mathbf{3}}, -\frac{1}{6})$
\hat{U}	\tilde{u}^c	u^c	3	$(-\frac{2}{3}, \mathbf{1}, \bar{\mathbf{3}}, -\frac{1}{6})$
\hat{L}	\tilde{L}	L	3	$(-\frac{1}{2}, \mathbf{2}, \mathbf{1}, -\frac{1}{2})$
\hat{E}	\tilde{e}^c	e^c	3	$(1, \mathbf{1}, \mathbf{1}, \frac{1}{2})$
$\hat{\nu}$	$\tilde{\nu}^c$	ν^c	3	$(0, \mathbf{1}, \mathbf{1}, \frac{1}{2})$
\hat{H}_d	H_d	\tilde{H}_d	1	$(-\frac{1}{2}, \mathbf{2}, \mathbf{1}, 0)$
\hat{H}_u	H_u	\tilde{H}_u	1	$(\frac{1}{2}, \mathbf{2}, \mathbf{1}, 0)$
$\hat{\eta}$	η	$\tilde{\eta}$	1	$(0, \mathbf{1}, \mathbf{1}, -1)$
$\hat{\bar{\eta}}$	$\bar{\eta}$	$\tilde{\bar{\eta}}$	1	$(0, \mathbf{1}, \mathbf{1}, 1)$

Table 1: Chiral superfields and their quantum numbers.

The superpotential is given by

$$\begin{aligned}
W = & Y_u^{ij} \hat{U}_i \hat{Q}_j \hat{H}_u - Y_d^{ij} \hat{D}_i \hat{Q}_j \hat{H}_d - Y_e^{ij} \hat{E}_i \hat{L}_j \hat{H}_d + \mu \hat{H}_u \hat{H}_d \\
& + Y_\nu^{ij} \hat{L}_i \hat{H}_u \hat{\nu}_j - \mu' \hat{\eta} \hat{\bar{\eta}} + Y_x^{ij} \hat{\nu}_i \hat{\eta} \hat{\nu}_j
\end{aligned} \tag{2.1}$$

and we have the additional soft SUSY-breaking terms:

$$\begin{aligned}
\mathcal{L}_{SB} = & \mathcal{L}_{MSSM} - \lambda_{\bar{B}} \lambda_{\bar{B}'} M_{BB'} - \frac{1}{2} \lambda_{\bar{B}'} \lambda_{\bar{B}} M_{B'} - m_\eta^2 |\eta|^2 - m_{\bar{\eta}}^2 |\bar{\eta}|^2 - m_{\nu, ij}^2 (\tilde{\nu}_i^c)^* \tilde{\nu}_j^c \\
& - \eta \bar{\eta} B_{\mu'} + T_\nu^{ij} H_u \tilde{\nu}_i^c \tilde{L}_j + T_x^{ij} \eta \tilde{\nu}_i^c \tilde{\nu}_j^c
\end{aligned} \tag{2.2}$$

i, j are generation indices. Without loss of generality one can take B_μ and $B_{\mu'}$ to be real. The extended gauge group breaks to $SU(3)_C \otimes U(1)_{em}$ as the Higgs fields and bileptons receive vacuum expectation values (*vevs*):

$$H_d^0 = \frac{1}{\sqrt{2}} (\sigma_d + v_d + i\phi_d), \quad H_u^0 = \frac{1}{\sqrt{2}} (\sigma_u + v_u + i\phi_u) \tag{2.3}$$

$$\eta = \frac{1}{\sqrt{2}} (\sigma_\eta + v_\eta + i\phi_\eta), \quad \bar{\eta} = \frac{1}{\sqrt{2}} (\sigma_{\bar{\eta}} + v_{\bar{\eta}} + i\phi_{\bar{\eta}}) \tag{2.4}$$

We define $\tan \beta' = \frac{v_\eta}{v_{\bar{\eta}}}$ in analogy to the ratio of the MSSM *vevs* ($\tan \beta = \frac{v_u}{v_d}$).

2.2 Gauge kinetic mixing

As already mentioned in the introduction, the presence of two Abelian gauge groups in combination with the given particle content gives rise to a new effect absent in the MSSM or other SUSY models with just one Abelian gauge group: the gauge kinetic mixing. This can be seen most easily by inspecting the matrix of the anomalous dimension, which at one loop is given by

$$\gamma_{ab} = \frac{1}{16\pi^2} \text{Tr} Q_a Q_b, \tag{2.5}$$

where the indices a and b run over all $U(1)$ groups and the trace runs over all fields charged under the corresponding $U(1)$ group.

For our model we obtain

$$\gamma = \frac{1}{16\pi^2} N \begin{pmatrix} 11 & 4 \\ 4 & 6 \end{pmatrix} N. \quad (2.6)$$

and we see that there are sizable off-diagonal elements. N contains the GUT normalization of the two Abelian gauge groups. We will take as in ref. [7] $\sqrt{\frac{3}{5}}$ for $U(1)_Y$ and $\sqrt{\frac{3}{2}}$ for $U(1)_{B-L}$, *i.e.* $N = \text{diag}(\sqrt{\frac{3}{5}}, \sqrt{\frac{3}{2}})$. Hence, we obtain finally

$$\gamma = \frac{1}{16\pi^2} \begin{pmatrix} \frac{33}{5} & 6\sqrt{\frac{2}{5}} \\ 6\sqrt{\frac{2}{5}} & 9 \end{pmatrix}. \quad (2.7)$$

Therefore, even if at the GUT scale the $U(1)$ kinetic mixing terms are zero, they are induced via RGE evaluation at lower scales. In practice it turns out that it is easier to work with non-canonical covariant derivatives instead of off-diagonal field-strength tensors such as in eq. (1.1). However, both approaches are equivalent [22]. Hence in the following, we consider covariant derivatives of the form

$$D_\mu = \partial_\mu - iQ_\phi^T G A \quad (2.8)$$

where Q_ϕ is a vector containing the charges of the field ϕ with respect to the two Abelian gauge groups, G is the gauge coupling matrix

$$G = \begin{pmatrix} g_{YY} & g_{YB} \\ g_{BY} & g_{BB} \end{pmatrix} \quad (2.9)$$

and A contains the gauge bosons $A = (A_\mu^Y, A_\mu^B)^T$.

As long as the two Abelian gauge groups are unbroken, we have still the freedom to perform a change of basis: $A = (A_\mu^Y, A_\mu^B) \rightarrow A' = ((A_\mu^Y)', (A_\mu^B)') = RA$ where R is an orthogonal matrix. It is possible to absorb this rotation of the gauge fields completely in the definition of the gauge couplings without the necessity of changing the charges, which can easily be seen using eq. (2.8)

$$Q_\phi^T G A = Q_\phi^T G (R^T R) A = Q_\phi^T (G R^T) A' = Q_\phi^T \tilde{G} A' \quad (2.10)$$

This freedom can be used to choose a basis such that electroweak precision data can be accommodated in an easy way. A convenient choice is the basis where $g_{BY} = 0$ as in this basis only the Higgs doublets contribute to the entries in the gauge boson mass matrix of the $U(1)_Y \otimes SU(2)_L$ sector and the impact of η and $\bar{\eta}$ is only in the

off-diagonal elements as discussed in section 2.4. Therefore we choose the following basis at the electroweak scale [23]:

$$g'_{YY} = \frac{g_{YY}g_{BB} - g_{YB}g_{BY}}{\sqrt{g_{BB}^2 + g_{BY}^2}} = g_1 \quad (2.11)$$

$$g'_{BB} = \sqrt{g_{BB}^2 + g_{BY}^2} = g_{BL} \quad (2.12)$$

$$g'_{YB} = \frac{g_{YB}g_{BB} + g_{BY}g_{YY}}{\sqrt{g_{BB}^2 + g_{BY}^2}} = \tilde{g} \quad (2.13)$$

$$g'_{BY} = 0 \quad (2.14)$$

This also leads to our condition for finding the GUT scale in the numerical analysis:

$$g_2 \equiv \frac{g_{YY}g_{BB} - g_{YB}g_{BY}}{\sqrt{g_{BB}^2 + g_{BY}^2}} \quad (2.15)$$

This is equivalent to a rotation of the general 2×2 gauge coupling matrix at each energy scale to the triangle form and using $g_1 = g_2$ as the GUT condition. Neglecting threshold corrections, this leads in the case of kinetic mixing to exactly the same GUT scale as in the MSSM [24].

Immediate interesting consequences of the gauge kinetic mixing arise in various sectors of the model as discussed in the subsequent sections: (i) it induces mixing at tree level between the H_u , H_d and η , $\bar{\eta}$; (ii) additional D-terms contribute to the mass matrices of the squarks and sleptons; (iii) off-diagonal soft-SUSY breaking terms for the gauginos are induced via RGE evolution [22, 25] with important consequences for the neutralino sector as discussed in section 3.4, even if at some fixed scale $M_{ab} = 0$ for $a \neq b$.

2.3 Tadpole equations

We find for the four minimization conditions at tree level

$$t_d = v_d \left(m_{H_d}^2 + |\mu|^2 + \frac{1}{8} (g_1^2 + g_2^2 + \tilde{g}^2) (v_d^2 - v_u^2) + \frac{1}{4} \tilde{g} g_{BL} (v_\eta^2 - v_{\bar{\eta}}^2) \right) - v_u B_\mu = 0 \quad (2.16)$$

$$t_u = v_u \left(m_{H_u}^2 + |\mu|^2 + \frac{1}{8} (g_1^2 + g_2^2 + \tilde{g}^2) (v_u^2 - v_d^2) + \frac{1}{4} \tilde{g} g_{BL} (v_\eta^2 - v_{\bar{\eta}}^2) \right) - v_d B_\mu = 0 \quad (2.17)$$

$$t_\eta = v_\eta \left(m_\eta^2 + |\mu'|^2 + \frac{1}{4} \tilde{g} g_{BL} (v_d^2 - v_u^2) + \frac{1}{2} g_{BL}^2 (v_\eta^2 - v_{\bar{\eta}}^2) \right) - v_{\bar{\eta}} B_{\mu'} = 0 \quad (2.18)$$

$$t_{\bar{\eta}} = v_{\bar{\eta}} \left(m_{\bar{\eta}}^2 + |\mu'|^2 + \frac{1}{4} \tilde{g} g_{BL} (v_u^2 - v_d^2) + \frac{1}{2} g_{BL}^2 (v_\eta^2 - v_{\bar{\eta}}^2) \right) - v_\eta B_{\mu'} = 0 \quad (2.19)$$

We solve them with respect to μ , B_μ , μ' and $B_{\mu'}$ as these parameters do not enter any of the RGEs of the other parameters. Using $x^2 = v_\eta^2 + v_{\bar{\eta}}^2$ and $v^2 = v_d^2 + v_u^2$ we

obtain

$$|\mu|^2 = \frac{1}{8} \left(\left(2\tilde{g}g_{BL}x^2 \cos(2\beta') - 4m_{H_d}^2 + 4m_{H_u}^2 \right) \sec(2\beta) - 4 \left(m_{H_d}^2 + m_{H_u}^2 \right) - \left(g_1^2 + \tilde{g}^2 + g_2^2 \right) v^2 \right) \quad (2.20)$$

$$B_\mu = -\frac{1}{8} \left(-2\tilde{g}g_{BL}x^2 \cos(2\beta') + 4m_{H_d}^2 - 4m_{H_u}^2 + \left(g_1^2 + \tilde{g}^2 + g_2^2 \right) v^2 \cos(2\beta) \right) \tan(2\beta) \quad (2.21)$$

$$|\mu'|^2 = \frac{1}{4} \left(-2 \left(g_{BL}^2 x^2 + m_\eta^2 + m_{\bar{\eta}}^2 \right) + \left(2m_\eta^2 - 2m_{\bar{\eta}}^2 + \tilde{g}g_{BL}v^2 \cos(2\beta) \right) \sec(2\beta') \right) \quad (2.22)$$

$$B_{\mu'} = \frac{1}{4} \left(-2g_{BL}^2 x^2 \cos(2\beta') + 2m_\eta^2 - 2m_{\bar{\eta}}^2 + \tilde{g}g_{BL}v^2 \cos(2\beta) \right) \tan(2\beta') \quad (2.23)$$

$M'_Z \simeq g_{BL}x$ as we will show in section 2.4 and, thus, we find an approximate relation between M'_Z and μ'

$$M_{Z'}^2 \simeq -2|\mu'|^2 + \frac{4(m_{\bar{\eta}}^2 - m_\eta^2 \tan^2 \beta') - v^2 \tilde{g}g_{BL} \cos \beta (1 + \tan \beta')}{2(\tan^2 \beta' - 1)} \quad (2.24)$$

A closer inspection of the system shows that either m_η^2 or $m_{\bar{\eta}}^2$ has to become negative to break $U(1)_{B-L}$. For both parameters, gauge couplings enter the RGEs, increasing their values when evolving from the GUT scale to the electroweak scale. The Yukawa couplings Y_ν and Y_x as well as the trilinear couplings T_ν and T_x lead to a decrease, but at the one-loop level they only affect the RGE for m_η^2 . However, neutrino data require $|Y_{\nu,ij}|$ to be very small in this model and thus they can be neglected for these considerations. Therefore, $m_{\bar{\eta}}$ will always be positive whereas m_η^2 can become negative for sufficient large Y_x and T_x .

We can roughly estimate the contribution of these couplings to the running value of m_η^2 by a one-step integration assuming mSUGRA-like GUT conditions (see sect. 2.8) to

$$\Delta m_\eta^2 \simeq -\frac{1}{4\pi^2} \text{Tr}(Y_x Y_x^\dagger) (3m_0^2 + A_0^2) \log \left(\frac{M_{GUT}}{M_{SUSY}} \right) \quad (2.25)$$

with $T_x \simeq A_0 Y_x$. Therefore, we expect that large values of m_0 and A_0 will be preferred, implying heavy sfermions. Moreover, $\tan \beta'$ has to be small and of $\mathcal{O}(1)$ in order to get a small denominator in the second term of eq. 2.24. One last comment concerning the effect of gauge kinetic mixing: g_{YB} is always negative below the GUT scale if it is zero at the GUT scale as can be seen by the following: for vanishing off-diagonal gauge couplings, the β -functions eqs. (B.17) and (B.16) will always be positive, *i.e.* g_{BY} and g_{YB} are driven negative. Using eq. (2.13), one can see that this also drives \tilde{g} negative. Therefore, the second term will give a positive contribution. From this point of view, one might expect that small m_0 for given $\tan \beta'$ would be sufficient to get the same size of $|\mu'|$. However, as can be seen in Fig. 1, where we plot the tree-level value of μ' in the $(m_0, \tan \beta')$ -plane for the cases with and without

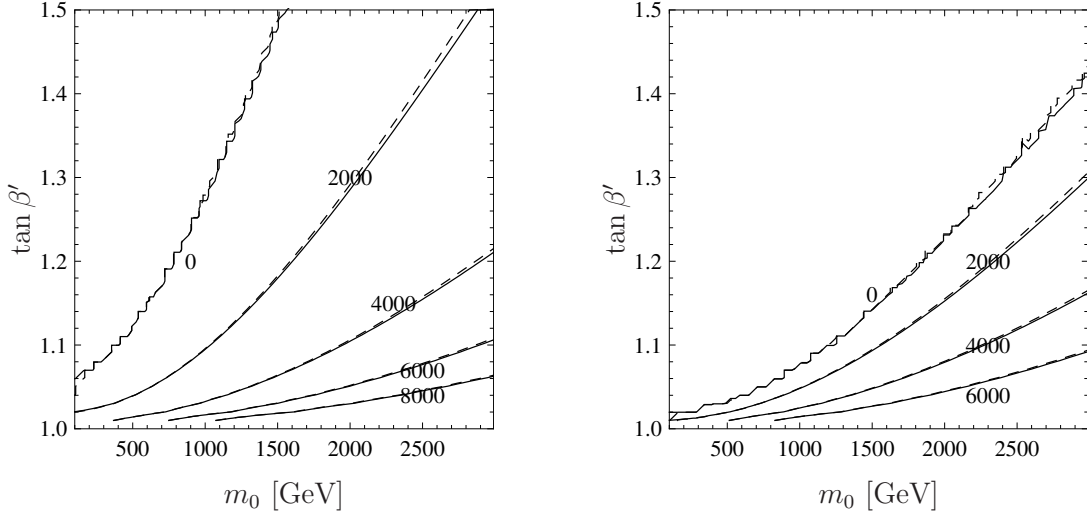


Figure 1: Contour plots of μ' at tree-level in the $(m_0, \tan \beta')$ -plane for $M_{Z'} = 2000$ GeV (left) and $M_{Z'} = 4000$ GeV (right). The other parameters are $M_{1/2} = 0.5$ TeV, $\tan(\beta) = 10$, $A_0 = 1.5$ TeV, $Y_{x,ii} = 0.42$. The full lines correspond to the case including gauge kinetic mixing, the dashed lines are without kinetic mixing.

kinetic mixing, the opposite effect takes place. The reason is the contribution of the kinetic mixing to the evaluation of m_η^2 and $m_{\bar{\eta}}^2$. One can also see in this figure that the upper limit of $\tan \beta'$ for a given value of m_0 decreases with increasing $M_{Z'}$ as expected. Even if one might get the impression from this figure that the effects of kinetic mixing are in general small as they slightly shift the region where breaking of $U(1)_{B-L}$ can occur, it will be shown later that it can have a significant impact on the masses.

For the numerical results we include one-loop corrections to eqs. (2.16)-(2.23) as well as for all masses. This is done by using the $\overline{\text{DR}}$ scheme and extending the MSSM results given in ref. [26] in a similar manner to the NMSSM case discussed in ref. [27]. We denote the one-loop contributions to the tadpole equations (2.16)-(2.19) by $\delta t_i^{(1)}$. The requirement of keeping the values of $\tan \beta$ and $\tan \beta'$ after including the loop corrections as well as the conditions

$$t_i + \delta t_i^{(1)} = 0 \quad \text{for } i = d, u, \eta, \bar{\eta} \quad (2.26)$$

lead to shifts of μ , B_μ , μ' and $B_{\mu'}$ compared to the values obtained by eqs. (2.20)-(2.23).

2.4 Gauge boson mixing

Due to the presence of the kinetic mixing terms, the B' boson mixes at tree level with the B and W^3 bosons. Requiring the conditions of eqs. (2.11)-(2.14) means

that the corresponding mass matrix reads, in the basis (B, W^3, B') ,

$$\begin{pmatrix} \frac{1}{4}g_1^2v^2 & -\frac{1}{4}g_1g_2v^2 & \frac{1}{4}g_1\tilde{g}v^2 \\ -\frac{1}{4}g_1g_2v^2 & \frac{1}{4}g_2^2v^2 & -\frac{1}{4}\tilde{g}g_2v^2 \\ \frac{1}{4}g_1\tilde{g}v^2 & -\frac{1}{4}\tilde{g}g_2v^2 & (g_{BL}^2x^2 + \frac{1}{4}\tilde{g}^2v^2) \end{pmatrix} \quad (2.27)$$

In the limit $\tilde{g} \rightarrow 0$ both sectors decouple and the upper 2×2 block is just the standard mass matrix of the neutral gauge bosons in EWSB. This mass matrix can be diagonalized by a unitary mixing matrix to get the physical mass eigenstates γ , Z and Z' . The rotation matrix can be expressed by two mixing angles Θ_W and Θ'_W as

$$\begin{pmatrix} B \\ W \\ B' \end{pmatrix} = \begin{pmatrix} \cos \Theta_W & \cos \Theta'_W \sin \Theta_W & -\sin \Theta_W \sin \Theta'_W \\ \sin \Theta_W & -\cos \Theta_W \cos \Theta'_W & \cos \Theta_W \sin \Theta'_W \\ 0 & \sin \Theta'_W & \cos \Theta'_W \end{pmatrix} \begin{pmatrix} \gamma \\ Z \\ Z' \end{pmatrix} \quad (2.28)$$

The third angle is zero due to the special form of this matrix. Θ'_W can be approximated by [28]

$$\tan 2\Theta'_W \simeq \frac{2\tilde{g}\sqrt{g_1^2 + g_2^2}}{\tilde{g}^2 + 16\left(\frac{x}{v}\right)^2 g_{BL}^2 - g_2^2 - g_1^2} \quad (2.29)$$

The exact eigenvalues of eq. (2.27) are given by

$$M_\gamma = 0 \quad (2.30)$$

$$M_{Z,Z'} = \frac{1}{8} \left((g_1^2 + g_2^2 + \tilde{g}^2)v^2 + 4g_{BL}^2x^2 \mp \sqrt{(g_1^2 + g_2^2 + \tilde{g}^2)^2v^4 - 8(g_1^2 + g_2^2)g_{BL}^2v^2x^2 + 16g_{BL}^4x^4} \right) \quad (2.31)$$

Expanding these formulas in powers of v^2/x^2 , we find up to first order:

$$M_Z = \frac{1}{4} (g_1^2 + g_2^2) v^2, \quad M_{Z'} = g_{BL}^2 x^2 + \frac{1}{4} \tilde{g}^2 v^2 \quad (2.32)$$

All parameters in eqs. (2.16)-(2.19) as well as in the following mass matrices are understood as running parameters at a given renormalization scale Q . Note that the *vevs* v_d and v_u are obtained from the running mass $M_Z(Q)$ of the Z boson, which is related to the pole mass M_Z through

$$M_Z^2(Q) = \frac{g_1^2 + g_2^2}{4} (v_u^2 + v_d^2) = M_Z^2 + \text{Re}\{\Pi_{ZZ}^T(M_Z^2)\}. \quad (2.33)$$

Here, Π_{ZZ}^T is the transverse self-energy of the Z . See for more details also ref. [26].

The mass of additional vector bosons as well as their mixing with the SM Z boson, which imply for example a deviation of the fermion couplings to the Z boson compared to SM expectations, is severely constrained by precision measurements

from the LEP experiments [29, 30, 31]. The bounds are on both the mass of the Z' and the mixing with the standard Z boson, where the latter is constrained by $|\sin(\Theta_{W'})| < 0.0002$. Using eq. (2.29) together with eq. (2.32) as well as the values of the running gauge couplings, a limit on the Z' mass of about 1.2 TeV is obtained. Taking in addition the bounds obtained from U , T and S parameters into account [32] one gets $\frac{M_{Z'}}{Q_e^{B-L} g_{B-L}} > 7.1$ TeV which for $g_{B-L} \simeq 0.52$ implies $M_{Z'} \gtrsim 1.8$ TeV. Therefore we have taken always $M_{Z'} \geq 2$ TeV. In this way we have also satisfied the most recent bounds obtained by the ATLAS and CMS [33].

2.5 The Higgs sector

In this section we present the tree-level formulas for the Higgs sector and we briefly discuss the main steps to include the one-loop corrections. The one-loop formulas and further details will be presented elsewhere [34].

2.5.1 Pseudoscalar Higgs bosons

It turns out that in this sector there is no mixing between the $SU(2)$ doublets and the bileptons at tree level and we obtain in the basis $(\phi_d, \phi_u, \phi_\eta, \phi_{\bar{\eta}})$:

$$m_{A,T}^2 = \begin{pmatrix} B_\mu \tan \beta & B_\mu & 0 & 0 \\ B_\mu & B_\mu \cot \beta & 0 & 0 \\ 0 & 0 & B_{\mu'} \tan \beta' & B_{\mu'} \\ 0 & 0 & B_{\mu'} & B_{\mu'} \cot \beta' \end{pmatrix}. \quad (2.34)$$

Obviously, both sectors decouple at tree level. This is a consequence of the fact that we assume that there is no CP violation in the Higgs sector, so the different D-term contributions cancel exactly. One obtains two physical states A^0 and A_η^0 with masses

$$m_{A^0}^2 = \frac{2B_\mu}{\sin 2\beta}, \quad m_{A_\eta^0}^2 = \frac{2B_{\mu'}}{\sin 2\beta'}. \quad (2.35)$$

A more detailed study of the pseudoscalar sector at one-loop, including the question if the block-diagonal form of the mass matrix in eq. (2.34) can be maintained at higher order, goes beyond the scope of this work and will be presented elsewhere [34].

2.5.2 Scalar Higgs bosons

In the scalar sector the gauge kinetic terms do induce a mixing between the $SU(2)$ doublet Higgs fields and the bileptons. The mass matrix reads at tree level in the

basis $(\sigma_d, \sigma_u, \sigma_\eta, \sigma_{\bar{\eta}})$:

$$m_{h,T}^2 = \begin{pmatrix} m_{A^0}^2 s_\beta^2 + \bar{g}^2 v_u^2 & -m_{A^0}^2 c_\beta s_\beta - \bar{g}^2 v_d v_u & \frac{\tilde{g} g_{BL}}{2} v_d v_\eta & -\frac{\tilde{g} g_{BL}}{2} v_d v_{\bar{\eta}} \\ -m_{A^0}^2 c_\beta s_\beta - \bar{g}^2 v_d v_u & m_{A^0}^2 c_\beta^2 + \bar{g}^2 v_d^2 & -\frac{\tilde{g} g_{BL}}{2} v_u v_\eta & \frac{\tilde{g} g_{BL}}{2} v_u v_{\bar{\eta}} \\ \frac{\tilde{g} g_{BL}}{2} v_d v_\eta & -\frac{\tilde{g} g_{BL}}{2} v_u v_\eta & m_{A_\eta}^2 c_{\beta'}^2 + g_{BL}^2 v_\eta^2 & -m_{A_\eta}^2 c_{\beta'} s_{\beta'} - g_{BL}^2 v_\eta v_{\bar{\eta}} \\ -\frac{\tilde{g} g_{BL}}{2} v_d v_{\bar{\eta}} & \frac{\tilde{g} g_{BL}}{2} v_u v_{\bar{\eta}} & -m_{A_\eta}^2 c_{\beta'} s_{\beta'} - g_{BL}^2 v_\eta v_{\bar{\eta}} & m_{A_\eta}^2 s_{\beta'}^2 + g_{BL}^2 v_{\bar{\eta}}^2 \end{pmatrix} \quad (2.36)$$

where we have defined $\bar{g}^2 = \frac{1}{4}(g_1^2 + g_2^2 + \tilde{g}^2)$, $c_x = \cos(x)$ and $s_x = \sin(x)$ ($x = \beta, \beta'$). The one-loop corrections are included by calculating the real part of the poles of the corresponding propagator matrices [26, 34]

$$\text{Det} [p_i^2 \mathbf{1} - m_{h,1L}^2(p^2)] = 0, \quad (2.37)$$

where

$$m_{h,1L}^2(p^2) = m_T^{2,h} - \Pi_{hh}(p^2). \quad (2.38)$$

Equation (2.37) has to be solved for each eigenvalue $p^2 = m_i^2$ which can be achieved in an iterative procedure.

2.5.3 The charged Higgs boson

At the tree level one finds that the charged Higgs boson mass has exactly the same form as in the MSSM:

$$m_{H^\pm}^2 = m_{A^0}^2 + m_W^2 \quad (2.39)$$

However, for the one-loop corrections one obtains additional contributions due to the kinetic gauge mixing [34].

2.6 Neutralinos

In the neutralino sector we find that the gauge kinetic effects lead to a mixing between the usual MSSM neutralinos with the additional states, similar to the mixing in the CP-even Higgs sector. In other words, were these to be neglected, both sectors would decouple. The mass matrix reads in the basis $(\lambda_{\tilde{B}}, \tilde{W}^0, \tilde{H}_d^0, \tilde{H}_u^0, \lambda_{\tilde{B}'}, \tilde{\eta}, \tilde{\bar{\eta}})$

$$m_{\tilde{\chi}^0} = \begin{pmatrix} M_1 & 0 & -\frac{1}{2}g_1 v_d & \frac{1}{2}g_1 v_u & \frac{1}{2}M_{BB'} & 0 & 0 \\ 0 & M_2 & \frac{1}{2}g_2 v_d & -\frac{1}{2}g_2 v_u & 0 & 0 & 0 \\ -\frac{1}{2}g_1 v_d & \frac{1}{2}g_2 v_d & 0 & -\mu & -\frac{1}{2}\tilde{g} v_d & 0 & 0 \\ \frac{1}{2}g_1 v_u & -\frac{1}{2}g_2 v_u & -\mu & 0 & \frac{1}{2}\tilde{g} v_u & 0 & 0 \\ \frac{1}{2}M_{BB'} & 0 & -\frac{1}{2}\tilde{g} v_d & \frac{1}{2}\tilde{g} v_u & M_B & -g_{BL} v_\eta & g_{BL} v_{\bar{\eta}} \\ 0 & 0 & 0 & 0 & -g_{BL} v_\eta & 0 & -\mu' \\ 0 & 0 & 0 & 0 & g_{BL} v_{\bar{\eta}} & -\mu' & 0 \end{pmatrix} \quad (2.40)$$

It is well known that for real parameters such a matrix can be diagonalized by an orthogonal mixing matrix N such that $N^* M_T^{\tilde{\chi}^0} N^\dagger$ is diagonal. For complex parameters one has to diagonalize $M_T^{\tilde{\chi}^0} (M_T^{\tilde{\chi}^0})^\dagger$. We obtain, in a straightforward generalization of the formulas given in [26], at the one-loop level

$$M_{1L}^{\tilde{\chi}^0}(p_i^2) = M_T^{\tilde{\chi}^0} - \frac{1}{2} \left[\Sigma_S^0(p_i^2) + \Sigma_S^{0,T}(p_i^2) + \left(\Sigma_L^{0,T}(p_i^2) + \Sigma_R^0(p_i^2) \right) M_T^{\tilde{\chi}^0} + M_T^{\tilde{\chi}^0} \left(\Sigma_R^{0,T}(p_i^2) + \Sigma_L^0(p_i^2) \right) \right], \quad (2.41)$$

where we have denoted the wave-function corrections by Σ_R^0 , Σ_L^0 and the direct one-loop contribution to the mass by Σ_S^0 .

In this model, for the chosen boundary conditions, the lightest supersymmetric particle (LSP), and therefore the dark matter candidate, is always either the lightest neutralino or the lightest sneutrino. The reason is that m_0 must be very heavy in order to solve the tadpole equations, and therefore all sfermions are heavier than the lightest neutralino, with the possible exception of the sneutrinos. As described in sec. 2.7 below, the splitting of the CP-even and CP-odd components of the sneutrinos can be very large, pushing the mass of the lighter eigenstate down even to the point of being lighter than the lightest neutralino. However, we have chosen to leave the investigation of such a scenario to future work, and we take only points with neutralino LSPs as our benchmark scenarios. Before leaving this topic, we note that BLV has a lightest sneutrino that is almost as light as the lightest neutralino. A neutralino LSP is in general a mixture of all seven gauge eigenstates. However, normally the character is dominated by only one or two constituents. In that context, we can distinguish the following extreme cases:

1. $M_1 \ll M_2, \mu, M_B, \mu'$: Bino-like LSP
2. $M_2 \ll M_1, \mu, M_B, \mu'$: Wino-like LSP
3. $\mu \ll M_1, M_2, M_B, \mu'$: Higgsino-like LSP
4. $M_B \ll M_1, M_2, \mu, \mu'$: BLino-like LSP
5. $\mu' \ll M_1, M_2, \mu, M_B$: Bileptino-like LSP

In addition, we will summarize the Bino- and Wino-like states, *i.e.* the states built by the gauginos of the MSSM, in the following often by ‘gaugino-like’. Note that this doesn’t include the BLino, the gaugino of the $B - L$ sector.

Although the gauge kinetic effects do lead to sizable effects in the spectrum, they are not large enough to lead to a large mixing between the usual MSSM-like states and the new ones. Therefore, we find that the LSP is either mainly a MSSM-like state or mainly an admixture between the BLino and the bileptinos. A discussion of the parameter space where the different characters appear is given in sec. 3.4.

2.7 Charginos and sfermions

For completeness we also give a short summary of the other sectors of the model. The chargino mass matrix at tree level is exactly the same as for the MSSM:

$$M_T^{\tilde{\chi}^+} = \begin{pmatrix} M_2 & \frac{1}{\sqrt{2}}g_2 v_u \\ \frac{1}{\sqrt{2}}g_2 v_d & \mu \end{pmatrix}. \quad (2.42)$$

This mass matrix is diagonalized by a biunitary transformation such that $U^* M_T^{\tilde{\chi}^+} V^\dagger$ is diagonal. The matrices U and V are obtained by diagonalizing $M_T^{\tilde{\chi}^+} (M_T^{\tilde{\chi}^+})^\dagger$ and $(M_T^{\tilde{\chi}^+})^* (M_T^{\tilde{\chi}^+})^T$, respectively. At the one-loop level, one has to add the self-energies [26]

$$M_{1L}^{\tilde{\chi}^+}(p_i^2) = M_T^{\tilde{\chi}^+} - \Sigma_S^+(p_i^2) - \Sigma_R^+(p_i^2) M_T^{\tilde{\chi}^+} - M_T^{\tilde{\chi}^+} \Sigma_L^+(p_i^2). \quad (2.43)$$

The mass matrices for the squarks and the charged sleptons are given in appendix A. At tree level, the differences compared to the MSSM are the additional D-terms in the diagonal entries. All complex scalar mass matrices are diagonalized by an unitary matrix Z

$$Z_\phi m_\phi^2 Z_\phi^\dagger = m_{\phi, \text{diag}}^2. \quad (2.44)$$

The corresponding mass matrices at the one-loop level are again obtained by taking into account the self-energy according to

$$m_{1L}^{2,\phi}(p_i^2) = m_T^{2,\phi} - \Pi_{\phi\phi}(p_i^2), \quad (2.45)$$

and the one-loop masses are obtained by calculating the poles of the real part of the propagator matrix.

We focus here on the sneutrino sector as it shows two distinct features compared to the MSSM. Firstly, it gets enlarged by the additional superpartners of the right-handed neutrinos. Secondly, even more drastically, a splitting between the real and imaginary parts of the sneutrino occurs resulting in twelve states: six scalar sneutrinos and six pseudoscalar ones [35, 36]. The origin of this splitting is the $Y_x^{ij} \hat{\nu}_i \hat{\eta} \hat{\nu}_j$ in the superpotential, eq. (2.1), which is a $\Delta L = 2$ operator. Therefore, we define

$$\tilde{\nu}_L^i = \frac{1}{\sqrt{2}} (\sigma_L^i + i\phi_L^i) \quad \tilde{\nu}_R^i = \frac{1}{\sqrt{2}} (\sigma_R^i + i\phi_R^i) \quad (2.46)$$

The 6×6 mass matrices of the CP-even and CP-odd sneutrinos can be written in the basis (σ_L, σ_R) respectively (ϕ_L, ϕ_R) as

$$m_{\nu_{R,I}}^2 = \Re \begin{pmatrix} m_{LL} & m_{RL}^T \\ m_{RL} & m_{RR} \end{pmatrix} \quad (2.47)$$

with

$$m_{LL} = \frac{1}{8} \left(\mathbf{1} \left((g_1^2 + g_2^2 + \tilde{g}^2) (-v_u^2 + v_d^2) + \tilde{g}g_B (-2v_{\tilde{\eta}}^2 + 2v_{\tilde{\eta}}^2 - v_u^2 + v_d^2) \right. \right. \\ \left. \left. + 2g_B^2 (-v_{\tilde{\eta}}^2 + v_{\tilde{\eta}}^2) \right) + 8m_l^2 + 4v_u^2 Y_\nu Y_\nu^\dagger \right) \quad (2.48)$$

$$m_{RL} = \frac{1}{4} \left(-2\sqrt{2}v_d\mu Y_\nu^\dagger + v_u \left(2\sqrt{2}T_\nu^T \pm 4v_{\tilde{\eta}} Y_x Y_\nu^\dagger \right) \right) \quad (2.49)$$

$$m_{RR} = \frac{1}{8} \left(\mathbf{1} \left(2g_B^2 (v_{\tilde{\eta}}^2 - v_{\tilde{\eta}}^2) - \tilde{g}g_B (-v_u^2 + v_d^2) \right) + 8m_\nu^2 + 2v_{\tilde{\eta}} \left(\mp 4\sqrt{2}Y_x \mu'^* \right) \right. \\ \left. + 4v_u^2 Y_\nu^T Y_\nu^* + 2v_{\tilde{\eta}} \left(\pm 4\sqrt{2}T_x + 8v_{\tilde{\eta}} Y_x Y_x^* \right) \right) \quad (2.50)$$

where we have assumed CP conservation. In the case of complex trilinear couplings, a mixing between the scalar and pseudoscalar particles occurs, resulting in 12 mixed states and consequently in a 12×12 mass matrix. In particular the term $\sim v_{\tilde{\eta}} Y_x \mu'^*$ is potentially large and induces a large mass splitting between the scalar and pseudoscalar states. Also the corresponding soft SUSY term $\sim v_{\tilde{\eta}} T_x$ can lead to a sizable mass splitting in the case of large $|A_0|$. As a side-remark we note that in such a case also the determinant of this matrix could become negative indicating the breaking of R-parity in a somewhat different way compared to the discussion in ref. [7]. However, here we will concentrate on the R-parity conserving case and discuss R-parity violation elsewhere [21].

2.8 Boundary conditions at the GUT scale

We will consider in the following a scenario motivated by minimal supergravity. This means that we assume a GUT unification of all soft-breaking scalar masses as well as a unification of all gaugino mass parameters

$$m_0^2 = m_{H_d}^2 = m_{H_u}^2 = m_{\tilde{\eta}}^2 = m_{\tilde{\eta}}^2 \quad (2.51)$$

$$m_0^2 \delta_{ij} = m_D^2 \delta_{ij} = m_U^2 \delta_{ij} = m_Q^2 \delta_{ij} = m_E^2 \delta_{ij} = m_L^2 \delta_{ij} = m_\nu^2 \delta_{ij} \quad (2.52)$$

$$M_{1/2} = M_1 = M_2 = M_3 = M_{\tilde{B}'} \quad (2.53)$$

Also, for the trilinear soft-breaking coupling, the ordinary mSUGRA conditions are assumed

$$T_i = A_0 Y_i, \quad i = e, d, u, x, \nu. \quad (2.54)$$

We do not fix the parameters μ, B_μ, μ' and $B_{\mu'}$ at the GUT scale but determine them from the tadpole equations. The reason is that they do not enter the RGEs of the other parameters and thus can be treated independently. The corresponding formulas are given in section 2.3.

In addition, we consider the mass of the Z' and $\tan \beta'$ as inputs and use the following set of free parameters

$$m_0, M_{1/2}, A_0, \tan \beta, \tan \beta', \text{sign}(\mu), \text{sign}(\mu'), M_{Z'}, Y_x \text{ and } Y_\nu. \quad (2.55)$$

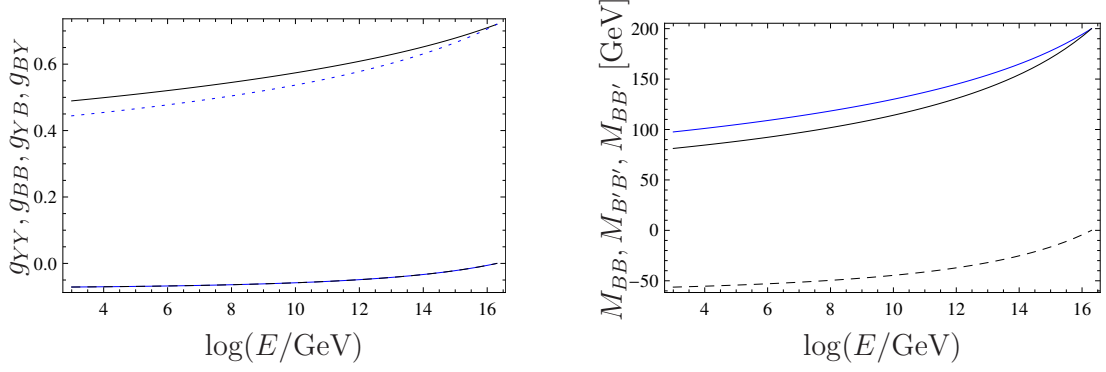


Figure 2: One-loop evaluation of the gauge couplings (left) and gaugino mass parameters (right) associated with the Abelian gauge groups. Blue color is used for g_{YY} & M_{BB} , black for g_{BB} & $M_{B'B'}$, dashed black for g_{YB} & $M_{BB'}$ and dashed blue for g_{BY} . The evolution of the two off-diagonal couplings hardly differs and thus the two lines nearly match.

Y_ν is constrained by neutrino data and must therefore be very small in comparison to the other couplings; thus it can be neglected in the following. Y_x can always be taken diagonal and thus effectively we have 9 free parameters and two signs.

Furthermore, we assume that there are no off-diagonal gauge couplings or gaugino mass parameters present at the GUT scale

$$g_{BY} = g_{YB} = 0 \quad (2.56)$$

$$M_{BB'} = 0 \quad (2.57)$$

This choice is motivated by the possibility that the two Abelian groups are a remnant of a larger product group which gets broken at the GUT scale as stated in the introduction. In that case g_{YY} and g_{BB} correspond to the physical couplings g_1 and g_{BL} , for which we assume a unification with g_2 :

$$g_1^{GUT} = g_2^{GUT} = g_{BL} . \quad (2.58)$$

where we have already taken into account the correct GUT normalization as discussed in section 2.2. In Fig. 2 we display the running of the gauge couplings and gaugino parameters in the Abelian sector to demonstrate the effect of the gauge kinetic mixing. The GUT scale has been set to $2 \cdot 10^{16}$ GeV where we have fixed $g_{YY} = g_{BB} = 0.72$ and $M_{BB} = M_{B'B'} = 200$ GeV. All off-diagonal parameters have been set to zero. Note that in particular $M_{BB'}$ becomes sizable at the electroweak scale.

3. Numerical results

All analytic expressions for masses, vertices, RGEs as well as one-loop corrections to the masses and tadpoles were calculated using the **SARAH** package [37, 38, 39]. For

the generic expressions, those of ref. [40] are used in the most general form respecting the complete flavour structure. In addition, gauge kinetic mixing effects in the RGEs are included using the extensions of ref. [22]. The loop corrections to all masses as well as to the tadpoles are derived in $\overline{\text{DR}}$ scheme and the 't Hooft gauge.

The numerical evaluation of the model is very similar to that of the default implementation of the MSSM in **SPheno** [41, 42]: as the starting point, the SM gauge and Yukawa couplings are determined using one-loop relations as given in ref. [26] which are extended to our model. The vacuum expectation values v_d and v_u are calculated with respect to the given value of $\tan \beta$ at M_Z , while v_η and $v_{\bar{\eta}}$ are derived from the input values of $M_{Z'}$ and $\tan \beta'$ at the SUSY scale.

The RGEs for the gauge and Yukawa couplings are evaluated up to the SUSY scale, where the input values of Y_ν and Y_x are set. Afterwards, a further evaluation of the RGEs up to the GUT scale takes place. After setting the boundary conditions all parameters are evaluated back to the SUSY scale. There, the one-loop-corrected SUSY masses are calculated using on-shell external momenta. These steps are iterated until the relative change of all masses between two iterations is below 10^{-4} .

3.1 Benchmark Points

For the numerical analysis in the following we have chosen five points in the constrained parameter space which have distinct features. An overview of these points is given in Tab. 2. A typical feature is that m_0 has to be in the TeV range to be consistent with the existing bounds on the Z' -mass.

BLI provides a neutralino LSP similar to the MSSM and also the lightest scalar Higgs is very similar to that of the MSSM and serves mainly to exemplify technical details. BLII demonstrates that it is possible to increase the Higgs mass of the MSSM-like light Higgs boson through a mixing with the new $B - L$ fields. BLIII has an LSP with a large Higgsino fraction that is difficult to reach within the MSSM. BLIV and BLV show two new dark matter candidates: a BLino and a bileptino LSP.

We have also chosen points which lead to SM-like Higgs masses in the preferred range of 123-126 GeV [43, 44]. As we will show in the following, the extended Higgs sector has an impact also on the MSSM Higgs masses. For instance, using the CMSSM parameters of BLI, the light Higgs would have a mass of 122.2 GeV, *i.e.* 1.5 GeV lighter. However, this effect will be smaller for points like BLIII or BLIV for which a larger mass splitting between the Higgs fields of both sectors is present. In this case, the light Higgs mass in the BLSSM agrees with that of the MSSM for the same parameters. One can also see that the branching ratios to two photons are always larger than in the SM except for BLIV, where the additional neutralinos are so light that $\text{Br}(h \rightarrow \tilde{\chi}_1^0 \tilde{\chi}_1^0) = 43.6\%$. This feature significantly softens, of course, the bounds on the Higgs mass.

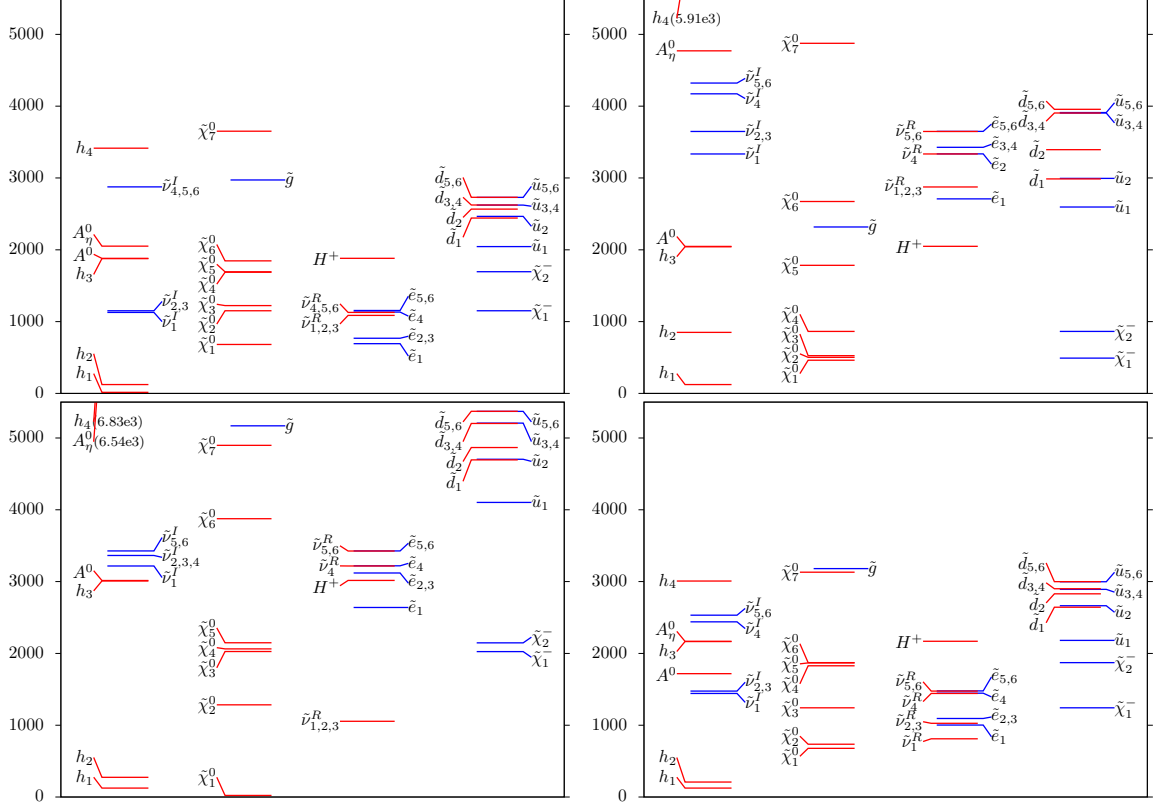


Figure 3: Spectrum of BLII (upper left figure), BLIII (upper right figure), BLIV (lower left figure) and BLV (lower right figure). All masses are given in GeV. The masses of the neutralinos and scalar Higgs fields are also given in table 2.

3.2 Precision of the mass calculation: the impact of kinetic mixing

Before we take a closer look on the Higgs and neutralino sector, we want to comment on the precision of the mass calculation. As already mentioned, we use two-loop RGEs and one-loop corrections to the masses. In addition, we take the feature of kinetic mixing into account which is often neglected in literature. To show the importance of the kinetic mixing and to compare the resulting mass spectrum of the $B - L$ model with the MSSM, we show in Tab. 3 the masses calculated at the one-loop level using one- or two-loop RGEs. For an easier comparison of the various effects, we fix the gauge the GUT scale to $2 \cdot 10^{16}$ GeV and the gauge couplings at the GUT scale to $g_1 = g_2 = g_3 = g_{BL} = 0.72$.

It can be seen that the most pronounced differences are in the neutralino and Higgs sectors. In case of sfermions and the heavier Higgs bosons the differences between the MSSM and BLSSM particle spectrum is about 1-2 percent and thus relatively small. They are larger in the charged slepton sector since here the additional $U(1)_{B-L}$ leads to larger effects. The main reason for the smallness of the differences is the required largeness of m_0 . Moreover, the D -term effects due to the extra $U(1)_{B-L}$ are also small as $\tan \beta'$ is close to 1. In the sneutrino sector the scalar

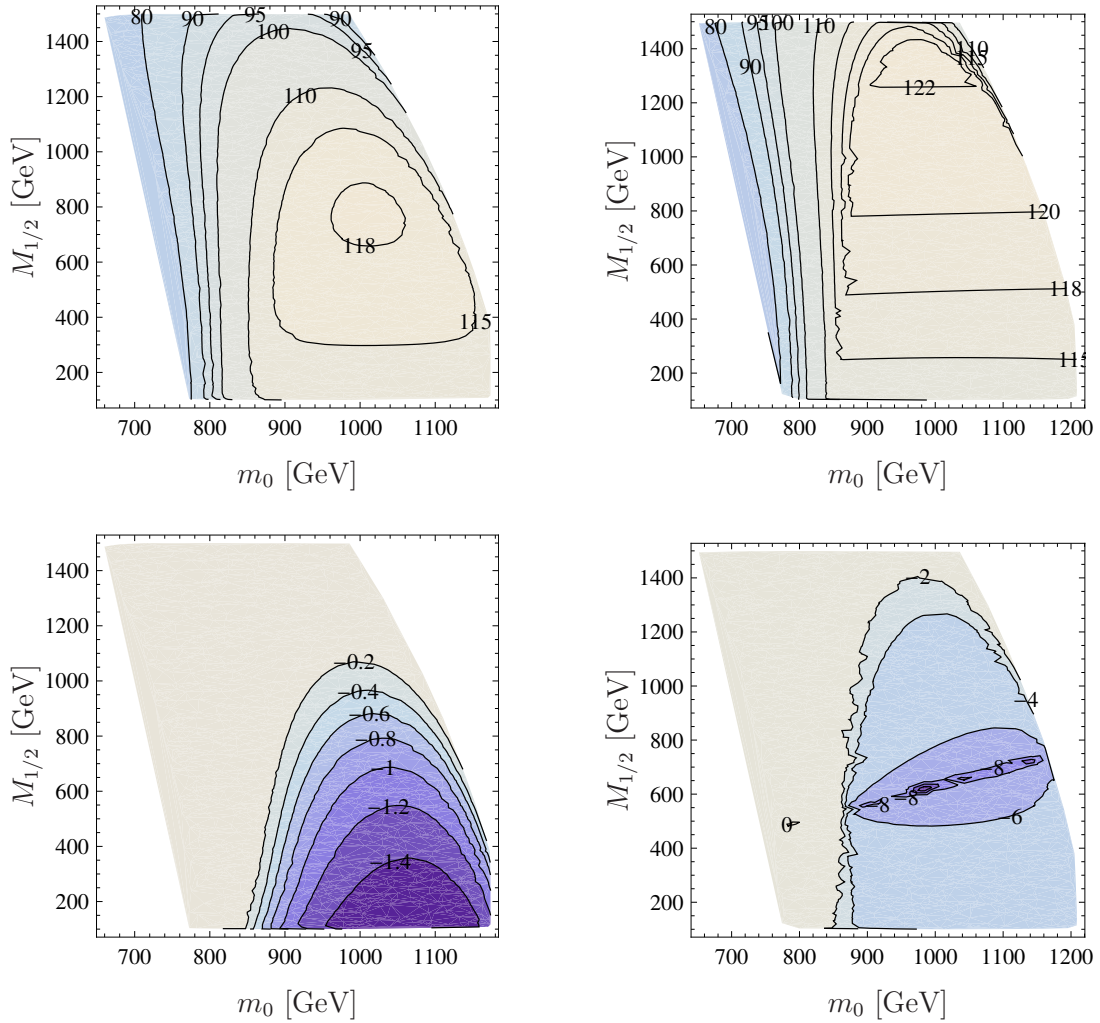


Figure 4: Mass of the lightest Higgs (first row) and the logarithm of the BLino fraction of the lightest Higgs (second row). The other parameters are those of BLI. First left: with kinetic mixing, right: without kinetic mixing.

and pseudoscalar particles behave quite differently: while the mass shifts in the pseudoscalar sector are rather moderate, the masses of the scalars change by more than 100 GeV. The cause for this is a partial cancellation for the given parameter point between the large positive terms in eq. (2.50), $m_\nu^2 + v_\eta Y_x Y_x^*$, and the large negative term $-4\sqrt{2}Y_x\mu'^*$ which is very sensitive to the exact values of all parameters at the SUSY scale. This also implies that kinetic mixing is particularly important for this sector and could even trigger R -parity violation [21].

In this table we also demonstrate that neglecting the gauge kinetic effects can have dramatic effects in the extended Higgs sector: the mass of h_2 state would be predicted to be about 20% larger.

Also in the neutralino sector there is quite some impact for the LSP masses

which would be wrong by about 10% if gauge kinetic terms were to be neglected. But also the properties of the lightest Higgs particle can change: we show in Fig. 4 a comparison between the mass and bilepton fraction of the lightest with and without kinetic mixing. It can be seen that the masses are clearly shifted while, of course, there is also huge difference of several orders in the bilepton fraction between both cases. While the bilepton contribution for MSSM-like scalars in the case without kinetic mixing is solely based on the mixing at one-loop level, the off-diagonal gauge couplings introduce already a tree-level mixing.

We turn now to the neutralino sector. When the lightest neutralino is bino- or Higgsino-like in this model, it shares the common features of the analogous neutralino in the MSSM. However, the masses differ at the SUSY scale for the same GUT scale parameters mainly as a consequence of gauge kinetic mixing in the gaugino sector which in our example amounts to shift of about 10 per-cent. This effect is especially important in the case of a bino LSP because the off-diagonal gaugino mass parameter $M_{BB'}$ can easily reach values of $\mathcal{O}(-50 \text{ GeV})$ (for $M_{1/2} \simeq 200 \text{ GeV}$) or even $\mathcal{O}(-150 \text{ GeV})$ (for $M_{1/2} \simeq 1000 \text{ GeV}$). For this purpose, we depict in the left column of Fig. 5 the mass of the lightest neutralino in the $(m_0, M_{1/2})$ -plane as well the BLino fraction. To point out again the importance of kinetic mixing, we show the same plots in the right column of 5 without the kinetic mixing. A shift of masses is clearly visible and also the admixture differs by several orders. The other parameters are the same as for Fig. 4.

For completeness we note that the differences between tree-level masses and loop-corrected masses are of similar size for the MSSM-particles. The R-sneutrinos receive somewhat larger loop corrections of about 3-4 per-cent compared to a few per-mille for the L-sneutrinos. However, interesting effects in the Higgs and neutralino sector can happen which we discuss in the next subsections.

3.3 The Higgs sector

In this section we concentrate on the Higgs sector and discuss new phenomenological aspects arising in the $B - L$ model. In Fig. 6 we show the lightest scalar Higgs mass in the $(m_0, M_{1/2})$ -plane. In addition, we give the bilepton fraction. The other input values are the same as for BLI. The nature of the second lightest Higgs is roughly complementary to the lightest one with respect to the ratio of the bilepton nature versus the Higgs doublet nature. The reason is that the mixing between the light states with the two heavy states, which have masses above a TeV, is quite small. Note that complete region shown is compatible with recent LHC data even though the mass of the second lightest Higgs boson is in most parts above 140 GeV, as it is mainly a bilepton with a small production cross section at the LHC.

Close to the border of the allowed regions in the $(m_0, M_{1/2})$ -plane, the lightest Higgs particles become bilepton-like. Not only can this be observed for a variation of m_0 and $M_{1/2}$ but also by adjusting $\tan \beta'$, as shown in Fig. 7 where we have fixed

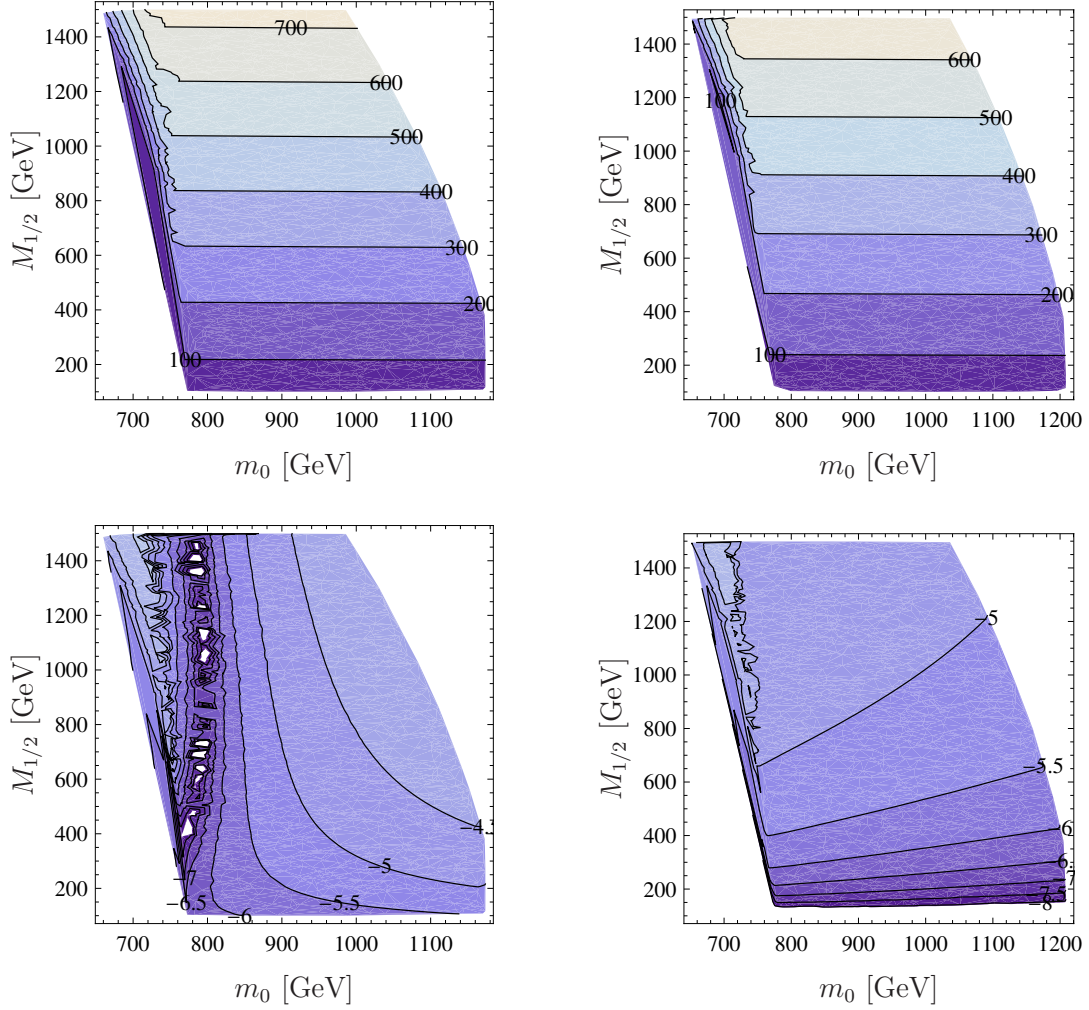


Figure 5: The $(m_0, M_{1/2})$ plane for a bino-LSP with kinetic mixing (left) and without (right). First row: mass of lightest neutralino. Second row: BLino fraction. The other parameters correspond to point BLI.

$m_0 = 1000$ GeV and $M_{1/2} = 500$ GeV. To understand this behavior we neglect gauge kinetic mixing for simplicity as then the bilepton sector decouples from the MSSM Higgs bosons. In this limit we obtain at tree level a similar formula for masses as for the MSSM Higgs bosons:

$$m_{1,2}^2 = \frac{1}{2} \left(m_{Z'}^2 + m_{A_\eta^0}^2 \mp \sqrt{(m_{Z'}^2 + m_{A_\eta^0}^2)^2 - 4m_{Z'}^2 m_{A_\eta^0}^2 \cos^2(2\beta')} \right) \quad (3.1)$$

Equations. (2.23) and (2.34) imply that for fixed $M_{Z'}$, $m_{A_\eta^0}^2$ shows a sizable dependence on $\tan \beta'$. We checked that very light bilepton-like Higgs scalars are not ruled out by experimental data using **HiggsBounds 3.6.1beta** [45, 46]. However, the mixing between the bilepton and the MSSM-like Higgs is rather small and thus the branching ratio $h_2 \rightarrow h_1 h_1$ is at most a few per-cent. Therefore, the main decay

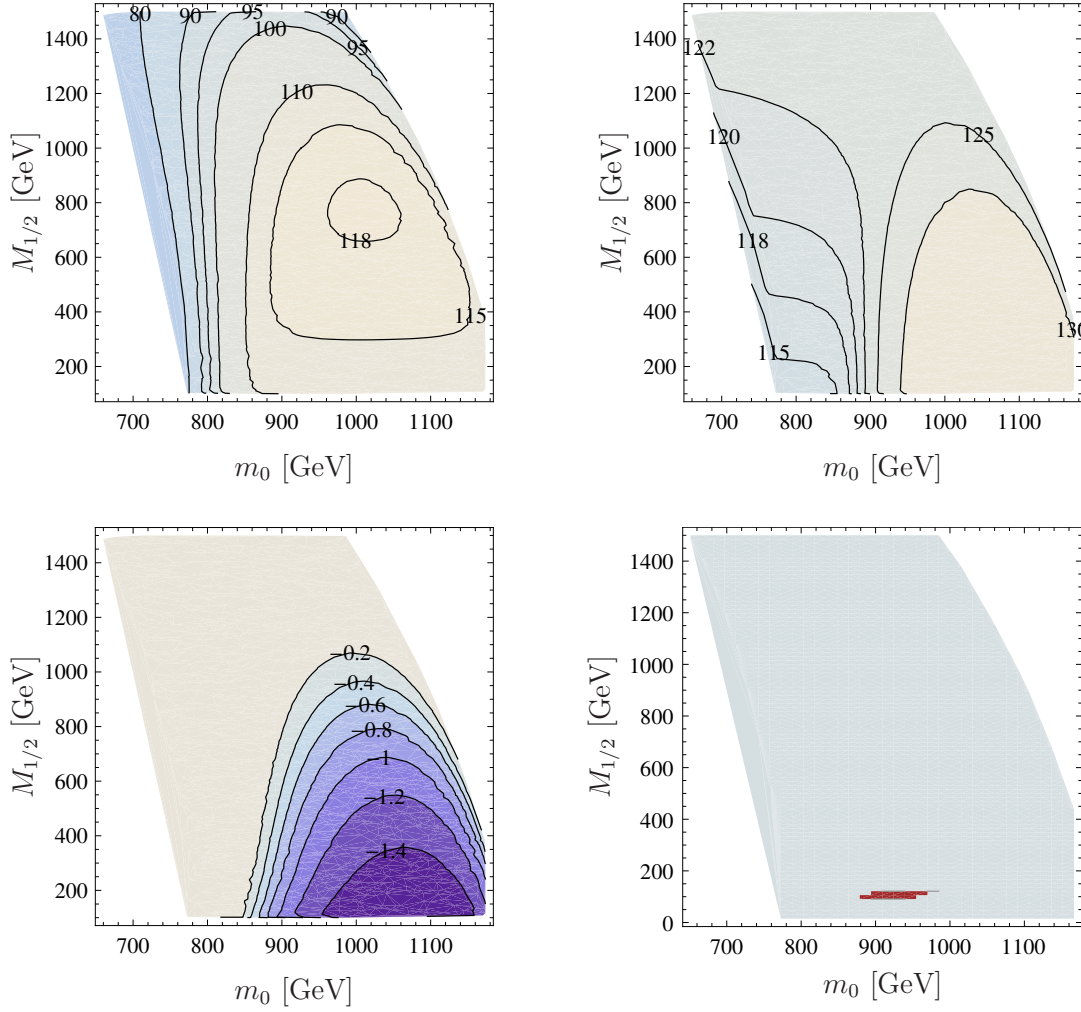


Figure 6: Mass of the lightest Higgs (first row on the left) and the second lightest Higgs (first row on the right), the logarithm of the bilepton fraction of the lightest Higgs (second row on the left) as well as the bounds from Higgs searches (second row on the right) in the $(m_0, M_{1/2})$ -plane. For the Higgs search the saturation of the tightest bound as calculated by HiggsBounds is shown. While the blue is still consistent with all data, the red area is excluded. The most stringent channels are $e^+e^- \rightarrow Zh_{1,2}, h_{1,2} \rightarrow b\bar{b}$ and $pp \rightarrow h_{1,2} \rightarrow W^+W^-$. The other parameters are as for point BLI.

channels of the doublet Higgs are still SM final states and the well-known bounds do hold. However, as can be seen also in Fig. 7, the mass of the MSSM-like Higgs bosons gets pushed to larger values for very light bilepton scalars. Such a behavior has already been observed in the literature when considering models with extended gauge symmetries [47, 48, 49, 50, 51, 52].

In Fig. 8 we take the point BLII and vary m_0 and $M_{1/2}$. We see that there is a sizable region where the lightest Higgs, being essentially a bilepton, has a mass of less than half of the second lightest, which is mainly like the MSSM h^0 . Even

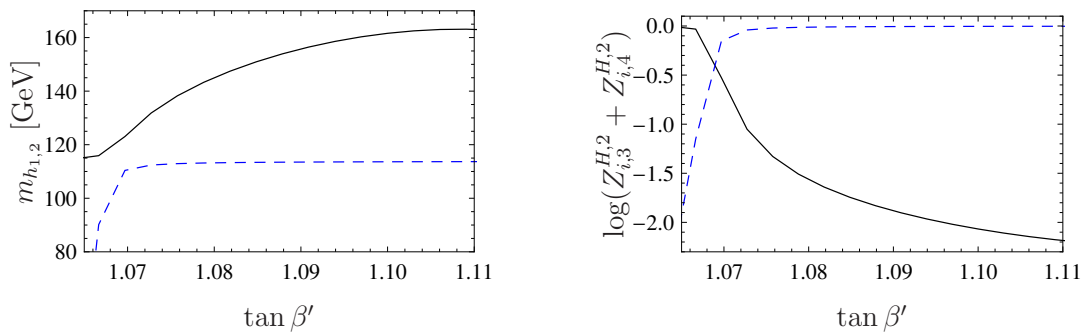


Figure 7: a) masses of two lightest scalars. b) doublet (dashed blue) and bilepton (black) fraction of lightest higgs as function of $\tan \beta'$. The other input parameters are as for point BLII, but with $m_0 = 2M_{1/2} = 1$ TeV

though the bilepton has only a small admixture of the doublet Higgs bosons, it is large enough to determine its main decay properties, which are mainly SM-like with respect to its decay into SM fermions.

Loop corrections Concerning the loop-corrections in the Higgs sector, the picture is often comparable with the MSSM: the lightest two Higgs bosons receive very large corrections. These are even larger for the chosen BLSSM point than in the MSSM. For the heavy doublet scalar as well as the charged and MSSM-like pseudoscalar Higgs, the differences between tree-level and one-loop masses are rather small and of the same size as in the MSSM. The neutrino Yukawa couplings don't play any role in this context because the correct explanation of neutrino data requires them to be very small. However, there are sizable loop corrections due to the large Y_x couplings similar to the top-stop contributions to the lighter MSSM-Higgs. For example, in the case of the BLIV scenario, m_{h_2} gets shifted from about 252 GeV at tree level to about 210 GeV at the one-loop level. This is a consequence of the mass hierarchy between fermions and bosons in the extended gauge/Higgs sector.

For completeness we note that in the Higgs sector one finds that the mass of the bilepton-like Higgs field vanishes at tree level in the limit $\tan \beta' \rightarrow 1$. Note, however, that $\tan \beta' = 1$ is a saddle point and not a minimum of the tree-level potential. This in turn implies that the loop corrections will be large compared to the tree level similar to as it is in the MSSM when considering there the limit $\tan \beta \rightarrow 1$. We explicitly demonstrate this in Fig. 9 where we compare the tree-level and one-loop masses of the two lightest Higgs fields, fixing the input parameters as in point BLII but varying $\tan \beta'$. This behavior is also reflected in the values of μ calculated from the one-loop and tree-level tadpole equations as shown in the right plot of Fig. 9. It can be understood from eq. (2.20): compared to $\cos(2\beta')$, all parameters and the one-loop corrections show only a very mild dependence on β' as $\tan \beta'$ has to be close to one. Therefore, the one-loop correction to the tadpole equation can be included

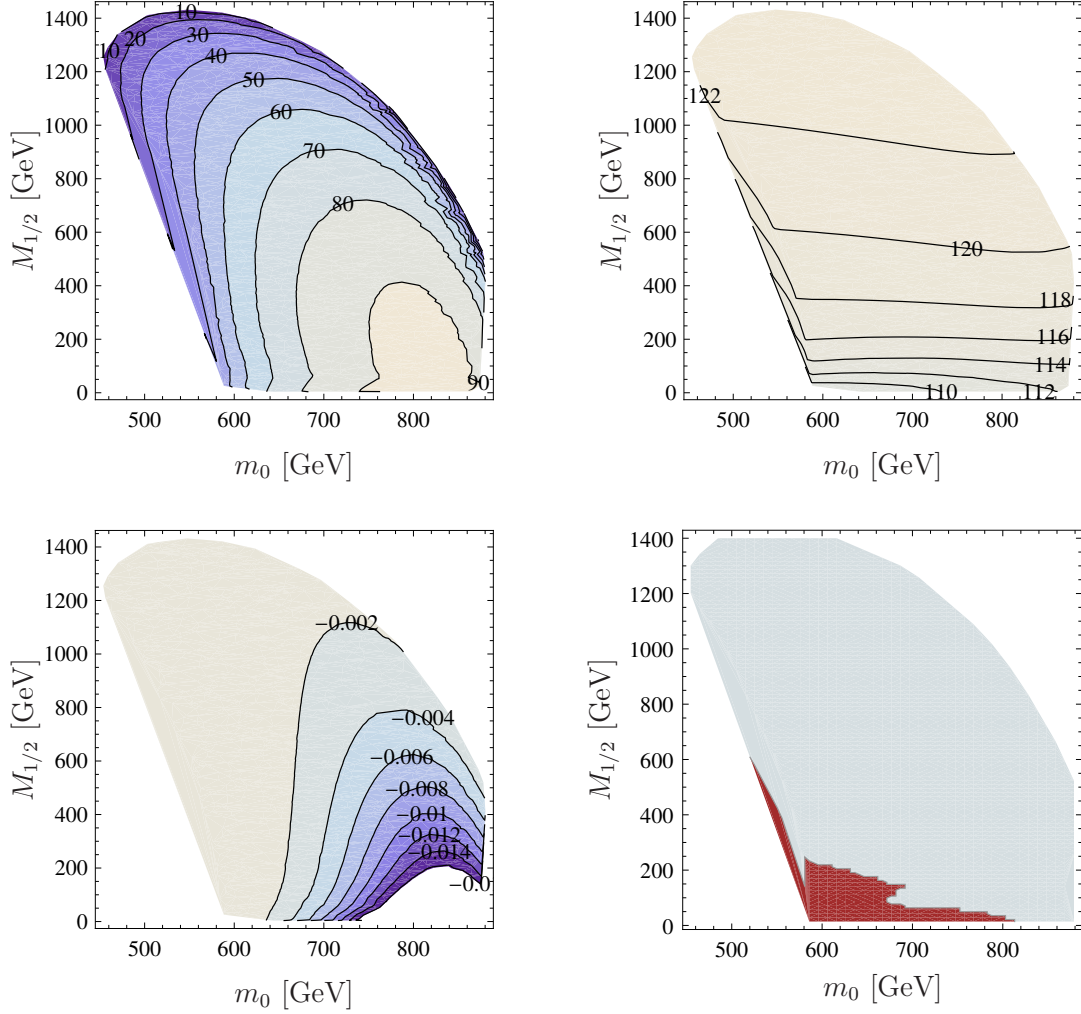


Figure 8: Mass of the two lightest Higgs fields (first row) as well as the logarithm of the bilepton fraction (left plot in second row) in the $(m_0, M_{1/2})$ -plane. The right plot in the second row shows the saturation of the tightest bound as calculated by **HiggsBounds**: the blue area is allowed, the red one excluded by Higgs searches. The most sensitive channels are $e^+e^- \rightarrow Zh_2, h_2 \rightarrow b\bar{b}$, $pp \rightarrow A^0 \rightarrow \tau\bar{\tau}$ and $pp \rightarrow h_2 \rightarrow W^+W^-$. The other parameters are based on BLII.

in the first term and effectively be absorbed in a redefinition of β' , denoted by $\tilde{\beta}'$, using the equation $\tilde{g}g_{BL}x^2 \cos(2\beta') + \frac{4(\delta t_u - \delta t_d)}{\sec(2\beta)} = \tilde{g}g_{BL}x^2 \cos(2\tilde{\beta}')$ with a shifted $\tilde{\beta}'$.

In Fig. 10 we show the masses of the two lightest Higgs fields for BLI with a variation of $M_{Z'}$. As expected the tree-level and one-loop mass of the lightest Higgs which consists mainly of the $SU(2)$ doublet is nearly independent of $M_{Z'}$. In contrast to that, the tree-level mass of the bilepton-like Higgs depends strongly on $M_{Z'}$. Furthermore, the one-loop corrections can be nearly of the order known from the MSSM for the doublet Higgs depending on the mass of the Z' . Also the sign of the correction can change depending on the mass ordering of Z' and the BLino-like

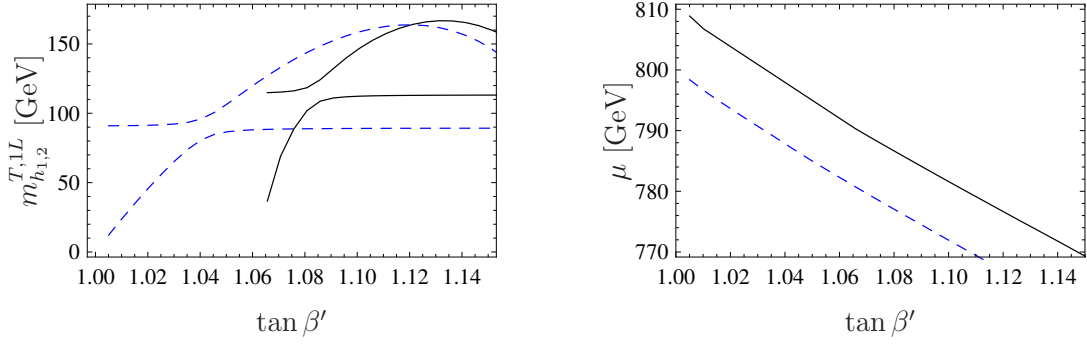


Figure 9: Left: mass of the lightest Higgs fields at one-loop level (black) and tree level (dashed blue). Right: value of μ calculated from the one-loop corrected tadpole equations (black) and the tadpole equations at tree level (dashed blue). The other input parameters correspond to those of Fig. 7

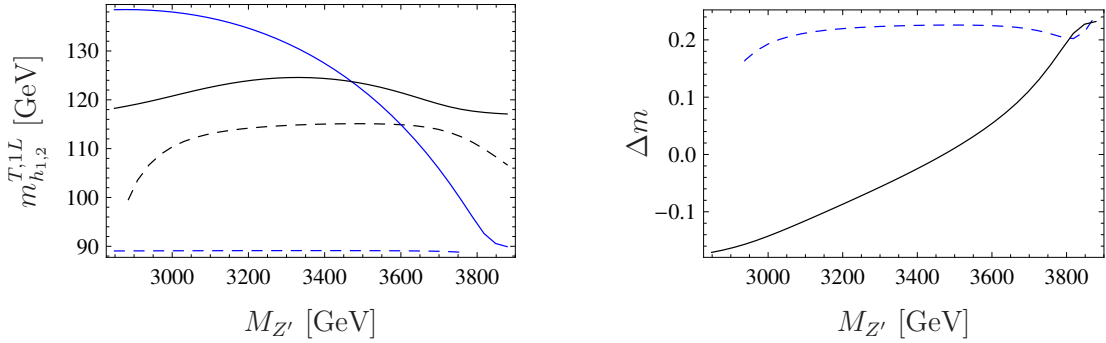


Figure 10: Left: masses of the lightest Higgs (dashed) and second lightest Higgs (solid) at one-loop level (black) and tree level (blue) for a variation of $M_{Z'}$. Right: relative difference between tree-level and one-loop mass for the lightest Higgs (dashed blue) and second lightest Higgs (solid black). The other input parameters correspond to point BLI.

neutralino.

3.4 The neutralino sector

Similarly to how it is in the CMSSM, the lightest neutralino is often bino-like and the main difference is, in this case, that the relation between the parameters at different scales gets changed due to the gauge kinetic mixing. Note that this holds even though the soft-breaking gaugino mass term $M_{B'}$ is always smaller than M_1 , because, at one-loop level and without kinetic mixing, the relation

$$\frac{M_{1/2}}{g_{GUT}^2} = \frac{M_1}{g_Y^2} = \frac{M_{B'}}{g_{BL}^2} \quad (3.2)$$

would hold and g_{BL} is always smaller than g_Y if unification at the GUT scale is assumed, as can be seen in eq. (2.7). However, usually there is a large mixing

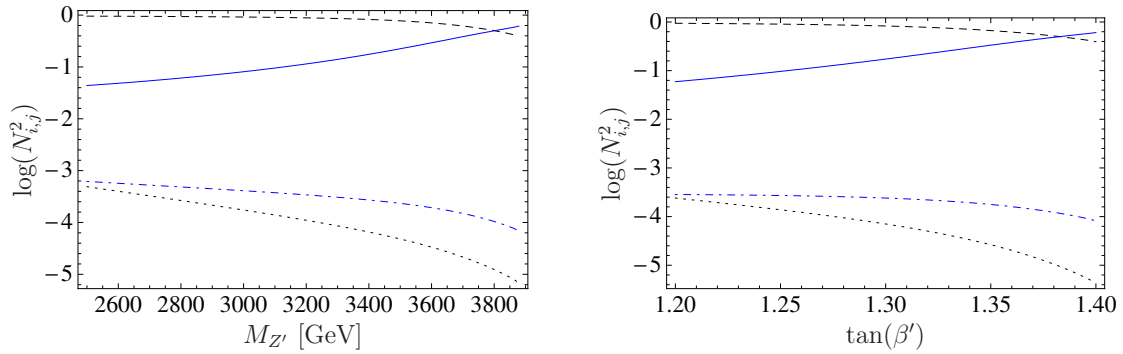


Figure 11: The content of the LSP depending on the $\tan\beta'$ (right) and $M_{Z'}$ (left). The other parameters are those of BLIII. The color code is as follows: gaugino fraction (dashed black), Higgsino fraction (blue), logarithm of the BLino fraction (dotted black) and bileptino fraction (dot-dashed blue).

between the BLino with the bileptinos, leading to heavy states. However, we will demonstrate that nevertheless regions exist where the lightest neutralino is BLino- or even bileptino-like. Therefore, a neutralino LSP can have four different natures in the BLSSM (bino, Higgsino, BLino, bileptino) in contrast to only two possibilities in the CMSSM. This can provide interesting features in the context of dark matter [34].

It is well known that in the MSSM, it is very hard to reach Higgsino fractions of the LSP larger than 50 per-cent: even in the focus point region this fraction hardly ever exceeds 30 per-cent. Only in a tiny region where $|\mu|$ gets close to 0, and which is excluded by LEP data, does it get larger than 50 per-cent. In contrast in our model new contributions show up in the formula for μ in eq. (2.20), in particular the term $\tilde{g}_{BL}x^2\cos(2\beta')$. Using universal boundary conditions it is in general negative and is particularly sizable for large $\tan\beta'$ and $M_{Z'}$. Therefore it is possible to increase the Higgsino fraction of the LSP by increasing these two parameters with fixed CMSSM parameters as shown in Fig. 11.

As mentioned above, the soft-breaking parameter $M_{B'}$ is always smaller than M_1 , but the large mixing between the BLino and the bileptino usually implies that the bino is still the LSP. However, there are regions where this mixing is small and the BLino becomes the LSP. In particular this happens if $\mu' \gg g_{BL}x \simeq M_{Z'}$ which happens either for large $|Y_x|$ or large m_0 , as this increases the difference $m_{\tilde{\eta}}^2 - m_{\tilde{\eta}'}^2$. As an example we show in Fig. 12 the dependence of μ' , the masses of all neutralinos and the content of the lightest on m_0 . As claimed, μ' grows with increasing m_0 leading to a larger mass splitting between the bileptino-like neutralinos and the others. For very large values of μ' , the bilepton fields are nearly decoupled and the nature of the LSP becomes BLino-like. In this case one has to check if one can obtain the correct value for the relic density. A principal possibility are resonances as there are two

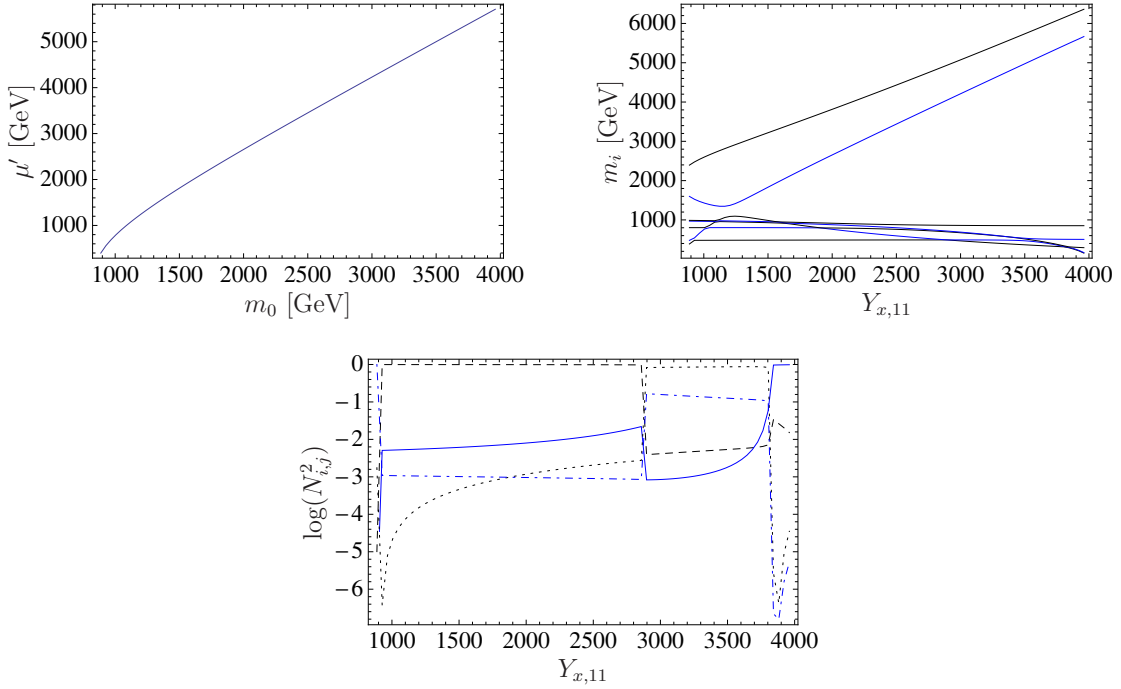


Figure 12: a) μ' as function of m_0 . b) masses of all neutralinos. c) content of the lightest neutralino: gaugino fraction (dashed black), Higgsino fraction (blue), logarithm of the BLino fraction (dotted black) and bileptino fraction (dot-dashed blue). The input parameters were those of BLIV but with $M_{1/2} = 1$ TeV.

light Higgs bosons and the LSP mass could easily be half of one of the Higgs masses. However, it still has to be checked if the corresponding couplings are sufficiently large, which however is beyond the scope of this paper.

We want to close the discussion of the BLino LSP with a remark about the importance of the loop corrections. It is well known that in the MSSM one gets a few per-cent corrections to the masses of sleptons, neutralinos and charginos [26]. In the model considered, the corrections are usually of a similar size. However, this doesn't apply for a light BLino because here loops contribute with rather heavy particles, in particular A_η^0 and the bileptino-like neutralinos. This is demonstrated by inspecting scenario BLIV. Varying $\tan \beta'$ we find that these corrections get larger the closer $\tan \beta'$ gets to one as can be seen in Fig. 13. At tree level one might then conclude that the LSP could be massless even for unified gaugino masses. This behavior can be roughly understood when neglecting gauge kinetic mixing as then the bileptinos and the BLino decouple from the MSSM neutralinos. In this limit it is thus sufficient to consider only the lower left 3×3 block of the neutralino mass matrix given in eq. (2.40). Taking $\tan \beta' = 1$ or equivalently $v_\eta \simeq v_{\bar{\eta}}$ we find for the LSP mass

$$\frac{1}{2}(M_B + \mu' - \sqrt{(M_B - \mu')^2 + 8(g_{BL}v_\eta)^2}) \quad (3.3)$$

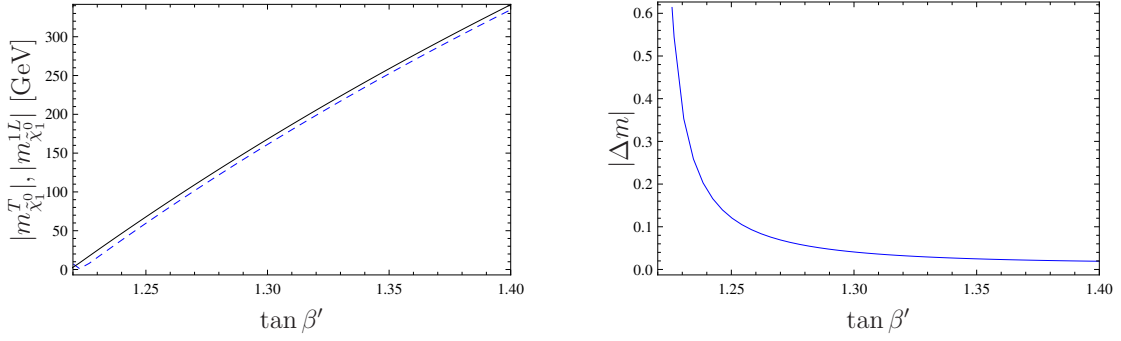


Figure 13: Left: mass of lightest neutralino at tree level (dashed blue) and one-loop level (black) for a variation of $\tan \beta'$. Right: relative size of the correction $|\Delta m| = |1 - \frac{m^T}{m^{1L}}|$. The input parameters are those of BLIV.

This expression can obviously be negative or positive for the same sign of μ' depending on the value of v_η . Although this gets changed at the one-loop level, it is still easy to obtain a dark matter candidate within the mass range preferred by direct detection experiments like DAMA [53, 54], CRESST [55] or Cogent [56].

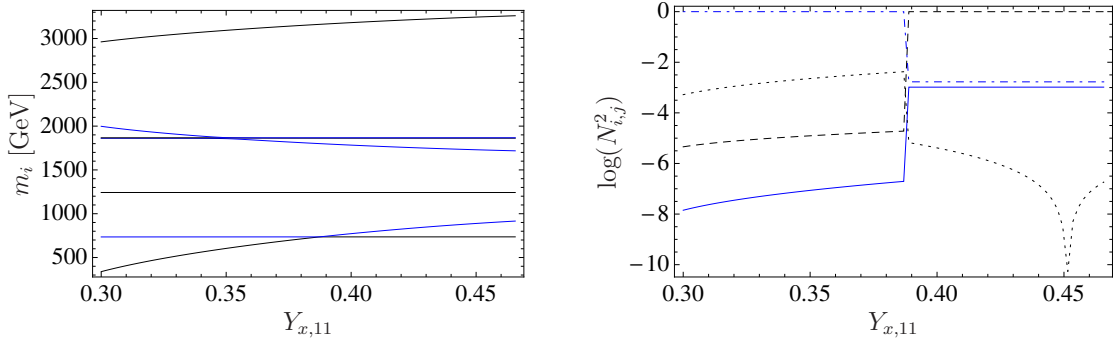


Figure 14: LSP with large bileptino fraction (benchmark scenario BLV): a) mass of neutralinos, b) neutralino content. The color code on the right-hand side is as follows: gaugino fraction (dashed black), Higgsino fraction (blue), logarithm of the BLino fraction (dotted black), bileptino fraction (dot-dashed blue).

Finally, we note that also a bileptino-like LSP can be obtained in this model. The necessary condition, $|\mu'|$ being smaller than $|\mu|$ and all gaugino mass parameters, can be obtained if the difference between m_η^2 and $m_{\tilde{\eta}}^2$ becomes small. This can be accommodated by adjusting the entries of Y_x . As an example, we show in Fig. 14 the masses of all neutralinos as well as the composition of the lightest neutralino as function of $Y_{x,11}$ while keeping all other values as in scenario BLV. Already a 10 per-cent decrease leads to a nearly a pure bileptino LSP and its mass depends strongly on $Y_{x,11}$. For larger values a level crossing takes place and the LSP becomes bino-like. In principal this coupling could be larger at the electroweak scale but then one would encounter a Landau pole below the GUT scale.

4. Conclusions and discussion

We have discussed in this paper the mass spectrum of the minimal $B - L$ extension of the MSSM taking universal boundary conditions at the GUT scale. We have calculated the spectrum using two-loop RGEs and the complete one-loop contributions to all masses, which are particularly important in the Higgs and neutralino sectors. Consistency with current bounds on the additional Z' implies that the scalar partners of the fermions are quite heavy in this scenario, except the sneutrinos can be light under certain conditions. However, this is a consequence of the taking the mass parameters of the sfermions equal to the ones in the extended Higgs sector. Relaxing this assumption allows for lighter non-sneutrino sfermions in addition to light sneutrinos.

It turns out that gauge kinetic mixing between the two Abelian gauge groups is quite important for Higgs bosons and neutralinos and it cannot be neglected. On one hand it leads to sizable shifts in the masses of up to 10 per-cent. On the other it induces tree-level mixing between the MSSM states and the states of the extended $B - L$ sector leading to important shifts in the nature of the corresponding particles. This holds in particular for the light Higgs bosons and the lightest neutralino. For example in the latter case we find regions in parameter space with light neutralinos as preferred by DAMA or COGENT. Moreover, the nature of the lightest neutralino can be quite different from the usual CMSSM, *e.g.* we have identified regions where it is either dominantly Higgsino-, BLino- or bileptino-like.

In the extended Higgs sector we find that one-loop corrections are not only important for the MSSM-like h^0 but also for the light bilepton field. This particle can be so light that the MSSM h^0 -like state can decay into two of them without conflicting with any of the known experimental results. However, in general we find that the corresponding branching ratio is at most a few per-cent.

Acknowledgements

We thank Pavel Fileviez Perez, Sogee Spinner, Lorenzo Basso, Stefano Morreti and Shaaban Khalil for interesting discussion. This work has been supported by the German Ministry of Education and Research (BMBF) under contract no. 05H09WWEF.

A. Mass matrices

Here we collect the tree-level formulas for the remaining sfermion mass matrices.

- **Mass matrix for Sleptons**, Basis: $(\tilde{e}_L, \tilde{e}_R)$

$$m_{\tilde{e}}^2 = \begin{pmatrix} m_{LL} & \frac{1}{\sqrt{2}}(v_d T_e - v_u \mu^* Y_e) \\ \frac{1}{\sqrt{2}}(v_d T_e^\dagger - v_u \mu Y_e^\dagger) & m_{RR} \end{pmatrix} \quad (\text{A.1})$$

$$m_{LL} = m_L^2 + \frac{v_d^2}{2} Y_e^\dagger Y_e + \frac{1}{8} \left((g_1^2 - g_2^2 + \tilde{g}^2 + \tilde{g}g_{BL})(v_d^2 - v_u^2) + 2(\tilde{g}g_{BL} + g_{BL}^2)(v_\eta^2 - v_{\bar{\eta}}^2) \right) \mathbf{1} \quad (\text{A.2})$$

$$m_{RR} = m_E^2 + \frac{v_d^2}{2} Y_e Y_e^\dagger + \frac{1}{8} \left((2g_1^2 + 2\tilde{g}^2 + \tilde{g}g_{BL})(v_u^2 - v_d^2) - 2(2\tilde{g}g_{BL} + g_{BL}^2)(v_\eta^2 - v_{\bar{\eta}}^2) \right) \mathbf{1} \quad (\text{A.3})$$

- **Mass matrix for Down-Squarks**, Basis: $(\tilde{d}_L, \tilde{d}_R)$

$$m_{\tilde{d}}^2 = \begin{pmatrix} m_{LL} & \frac{1}{\sqrt{2}}(v_d T_d - v_u \mu^* Y_d) \\ \frac{1}{\sqrt{2}}(v_d T_d^\dagger - v_u \mu Y_d^\dagger) & m_{RR} \end{pmatrix} \quad (\text{A.4})$$

$$m_{LL} = m_Q^2 + \frac{v_d^2}{2} Y_d^\dagger Y_d + \frac{1}{24} \left((g_1^2 + 3g_2^2 + \tilde{g}^2 + \tilde{g}g_{BL})(v_u^2 - v_d^2) + 2(g_{BL}^2 + \tilde{g}g_{BL})(v_\eta^2 - v_{\bar{\eta}}^2) \right) \mathbf{1} \quad (\text{A.5})$$

$$m_{RR} = m_D^2 + \frac{v_d^2}{2} Y_d Y_d^\dagger + \frac{1}{24} \left(-(2g_1^2 + 2\tilde{g}^2 - \tilde{g}g_{BL})(v_d^2 - v_u^2) + 2(g_{BL}^2 - 2\tilde{g}g_{BL})(v_\eta^2 - v_{\bar{\eta}}^2) \right) \mathbf{1} \quad (\text{A.6})$$

- **Mass matrix for Up-Squarks**, Basis: $(\tilde{u}_L, \tilde{u}_R)$

$$m_{\tilde{u}}^2 = \begin{pmatrix} m_{LL} & \frac{1}{\sqrt{2}}(v_u T_u - v_d \mu^* Y_u) \\ \frac{1}{\sqrt{2}}(v_u T_u^\dagger - v_d \mu Y_u^\dagger) & m_{RR} \end{pmatrix} \quad (\text{A.7})$$

$$m_{LL} = m_Q^2 + \frac{v_u^2}{2} Y_u^\dagger Y_u + \frac{1}{24} \left((g_1^2 - 3g_2^2 + \tilde{g}^2 + \tilde{g}g_{BL})(v_u^2 - v_d^2) + 2(\tilde{g}g_{BL} + g_{BL}^2)(v_\eta^2 - v_{\bar{\eta}}^2) \right) \mathbf{1} \quad (\text{A.8})$$

$$m_{RR} = m_U^2 + \frac{v_u^2}{2} Y_u Y_u^\dagger + \frac{1}{24} \left(2(g_{BL}^2 + 4\tilde{g}g_{BL})(v_\eta^2 - v_{\bar{\eta}}^2) + (4g_1^2 + 4\tilde{g}^2 + \tilde{g}g_{BL})(v_d^2 - v_u^2) \right) \mathbf{1} \quad (\text{A.9})$$

B. RGEs

The calculation of the renormalization group equations performed by **SARAH** is based on the generic expression of [40]. In addition, the results of [22] are used to include the effect of kinetic mixing.

The β functions for the parameters of a general superpotential written as

$$W(\phi) = \frac{1}{2} \mu^{ij} \phi_i \phi_j + \frac{1}{6} Y^{ijk} \phi_i \phi_j \phi_k \quad (\text{B.1})$$

can be easily obtained from the shown results for the anomalous dimensions by using the relations [57, 58]

$$\beta_Y^{ijk} = Y^{p(ij} \gamma_p^{k)} , \quad (\text{B.2})$$

$$\beta_\mu^{ij} = \mu^{p(i} \gamma_p^{j)} . \quad (\text{B.3})$$

For the results of the other parameters as well as for the two-loop results which we skip here because of their length we suggest to use the function `CalcRGEs []` of `SARAH` with the model files shown in appendix C.

B.1 Anomalous dimensions

$$\begin{aligned} \gamma_{\hat{q}}^{(1)} &= Y_d^\dagger Y_d + Y_u^\dagger Y_u \\ &\quad - \frac{1}{60} \left(2(g_{YY}^2 + g_{YB}^2) + 2\sqrt{10}(g_{YY}g_{BY} + g_{YB}g_{BB}) + 5(18g_2^2 + 32g_3^2 + g_{BB}^2 + g_{BY}^2) \right) \mathbf{1} \end{aligned} \quad (\text{B.4})$$

$$\begin{aligned} \gamma_{\hat{l}}^{(1)} &= Y_e^\dagger Y_e + Y_\nu^* Y_\nu^T \\ &\quad - \frac{3}{20} \left(2(g_{YY}^2 + g_{YB}^2) + 2\sqrt{10}(g_{YY}g_{BY} + g_{YB}g_{BB}) + 5(2g_2^2 + g_{BB}^2 + g_{BY}^2) \right) \mathbf{1} \end{aligned} \quad (\text{B.5})$$

$$\gamma_{\hat{H}_d}^{(1)} = 3\text{Tr}(Y_d Y_d^\dagger) + \text{Tr}(Y_e Y_e^\dagger) - \frac{3}{10} (5g_2^2 + g_{YY}^2 + g_{YB}^2) \quad (\text{B.6})$$

$$\gamma_{\hat{H}_u}^{(1)} = 3\text{Tr}(Y_u Y_u^\dagger) + \text{Tr}(Y_\nu Y_\nu^\dagger) - \frac{3}{10} (5g_2^2 + g_{YY}^2 + g_{YB}^2) \quad (\text{B.7})$$

$$\begin{aligned} \gamma_{\hat{d}}^{(1)} &= 2Y_d^* Y_d^T \\ &\quad + \frac{1}{60} \left(4\sqrt{10}(g_{YY}g_{BY} + g_{YB}g_{BB}) - 5(32g_3^2 + g_{BB}^2 + g_{BY}^2) - 8(g_{YY}^2 + g_{YB}^2) \right) \mathbf{1} \end{aligned} \quad (\text{B.8})$$

$$\begin{aligned} \gamma_{\hat{u}}^{(1)} &= 2Y_u^* Y_u^T \\ &\quad - \frac{1}{60} \left(32(g_{YY}^2 + g_{YB}^2) + 5(32g_3^2 + g_{BB}^2 + g_{BY}^2) + 8\sqrt{10}(g_{YY}g_{BY} + g_{YB}g_{BB}) \right) \mathbf{1} \end{aligned} \quad (\text{B.9})$$

$$\gamma_{\hat{e}}^{(1)} = 2Y_e^* Y_e^T - \frac{3}{20} \left(4\sqrt{10}(g_{YY}g_{BY} + g_{YB}g_{BB}) + 5(g_{BB}^2 + g_{BY}^2) + 8(g_{YY}^2 + g_{YB}^2) \right) \mathbf{1} \quad (\text{B.10})$$

$$\gamma_{\hat{\nu}}^{(1)} = 2Y_\nu^\dagger Y_\nu + 2(Y_x^\dagger Y_x + Y_x^* Y_x) - \frac{3}{4} (g_{BB}^2 + g_{BY}^2) \mathbf{1} \quad (\text{B.11})$$

$$\gamma_{\hat{\eta}}^{(1)} = -3(g_{BB}^2 + g_{BY}^2) + 2\text{Tr}(Y_x Y_x^\dagger) \quad (\text{B.12})$$

$$\gamma_{\hat{\hat{\eta}}}^{(1)} = -3(g_{BB}^2 + g_{BY}^2) \quad (\text{B.13})$$

B.2 Gauge Couplings

We give here and in the subsequent section the beta functions for the RGEs of the gauge couplings and gaugino mass parameters in a basis independent way as the off-diagonal values for the $U(1)$ gauge couplings and gaugino mass parameters are generated due to RGE effects.

$$\begin{aligned}\beta_{g_{YY}}^{(1)} = & \frac{3}{5} \left(11g_{YY}^3 + 4\sqrt{10}g_{YY}^2g_{BY} + g_{YY} \left(11g_{YB}^2 + 15g_{BY}^2 + 2\sqrt{10}g_{YB}g_{BB} \right) \right. \\ & \left. + g_{YB} \left(15g_{BB} + 2\sqrt{10}g_{YB} \right) g_{BY} \right) \quad (B.14)\end{aligned}$$

$$\begin{aligned}\beta_{g_{BB}}^{(1)} = & \frac{3}{5} \left(11g_{YB}^2g_{BB} + 4\sqrt{10}g_{YB}g_{BB}^2 + 15g_{BB}^3 + 11g_{YY}g_{YB}g_{BY} + 2\sqrt{10}g_{YY}g_{BB}g_{BY} \right. \\ & \left. + 2\sqrt{10}g_{YB}g_{BY}^2 + 15g_{BB}g_{BY}^2 \right) \quad (B.15)\end{aligned}$$

$$\begin{aligned}\beta_{g_{YB}}^{(1)} = & \frac{3}{5} \left(g_{YY} \left(15g_{BB} + 2\sqrt{10}g_{YB} \right) g_{BY} + g_{YY}^2 \left(11g_{YB} + 2\sqrt{10}g_{BB} \right) \right. \\ & \left. + g_{YB} \left(11g_{YB}^2 + 15g_{BB}^2 + 4\sqrt{10}g_{YB}g_{BB} \right) \right) \quad (B.16)\end{aligned}$$

$$\begin{aligned}\beta_{g_{BY}}^{(1)} = & \frac{3}{5} \left(11g_{YY}^2g_{BY} + g_{YY} \left(11g_{YB}g_{BB} + 2\sqrt{10} \left(2g_{BY}^2 + g_{BB}^2 \right) \right) \right. \\ & \left. + g_{BY} \left(15 \left(g_{BB}^2 + g_{BY}^2 \right) + 2\sqrt{10}g_{YB}g_{BB} \right) \right) \quad (B.17)\end{aligned}$$

$$\beta_{g_2}^{(1)} = g_2^3 \quad (B.18)$$

$$\beta_{g_3}^{(1)} = -3g_3^3 \quad (B.19)$$

B.3 Gaugino Mass Parameters

$$\begin{aligned}\beta_{M_1}^{(1)} = & \frac{6}{5} \left(11g_{YY}^2M_1 + g_{BY} \left(15g_{BB}M_{BB'} + 15g_{BY}M_1 + 2\sqrt{10}g_{YB}M_{BB'} \right) \right. \\ & \left. + g_{YY} \left(11g_{YB}M_{BB'} + 2\sqrt{10}g_{BB}M_{BB'} + 4\sqrt{10}g_{BY}M_1 \right) \right) \quad (B.20)\end{aligned}$$

$$\beta_{M_2}^{(1)} = 2g_2^2M_2 \quad (B.21)$$

$$\beta_{M_3}^{(1)} = -6g_3^2M_3 \quad (B.22)$$

$$\begin{aligned}\beta_{M_B}^{(1)} = & \frac{6}{5} \left(11g_{YB}^2M_B + 15g_{BB} \left(g_{BB}M_B + g_{BY}M_{BB'} \right) + \right. \\ & \left. 2\sqrt{10}g_{YB} \left(2g_{BB}M_B + g_{BY}M_{BB'} \right) + g_{YY} \left(11g_{YB} + 2\sqrt{10}g_{BB} \right) M_{BB'} \right) \quad (B.23)\end{aligned}$$

$$\begin{aligned}\beta_{M_{BB'}}^{(1)} = & \frac{3}{5} \left(11g_{YY}^2M_{BB'} + 11g_{YB}^2M_{BB'} + 2\sqrt{10}g_{YB} \left(2g_{BB}M_{BB'} + g_{BY} \left(M_1 + M_B \right) \right) + \right. \\ & \left. 15 \left(g_{BB}^2M_{BB'} + g_{BB}g_{BY} \left(M_1 + M_B \right) + g_{BY}^2M_{BB'} \right) \right. \\ & \left. + g_{YY} \left(11g_{YB} \left(M_1 + M_B \right) + 2\sqrt{10} \left(2g_{BY}M_{BB'} + g_{BB} \left(M_1 + M_B \right) \right) \right) \right) \quad (B.24)\end{aligned}$$

C. Model files for SARAH

Below we list the model files used for SARAH to study the model presented in this paper. Using this one can generate the Fortran code for the **SPheno** extension to reproduce the results presented. These files will also become part of the public SARAH package in near future.

C.1 B-L-SSM.m

```
(*-----*)
(*   Particle Content   *)
(*-----*)

(* Gauge Superfields *)

Gauge[[1]]={B,   U[1], hypercharge, g1,False};
Gauge[[2]]={WB, SU[2], left,      g2,True};
Gauge[[3]]={G,   SU[3], color,     g3,False};
Gauge[[4]]={Bp,  U[1], BminusL,   g1p, False};

(* Chiral Superfields *)

Fields[[1]] = {{uL, dL}, 3, q, 1/6, 2, 3, 1/6};
Fields[[2]] = {{vL, eL}, 3, l, -1/2, 2, 1, -1/2};
Fields[[3]] = {{Hd0, Hd1}, 1, Hd, -1/2, 2, 1, 0};
Fields[[4]] = {{Hup, Hu0}, 1, Hu, 1/2, 2, 1, 0};

Fields[[5]] = {conj[dR], 3, d, 1/3, 1, -3, -1/6};
Fields[[6]] = {conj[uR], 3, u, -2/3, 1, -3, -1/6};
Fields[[7]] = {conj[eR], 3, e, 1, 1, 1, 1/2};
Fields[[8]] = {conj[vR], 3, vR, 0, 1, 1, 1/2};

Fields[[9]] = {C10, 1, C1, 0, 1, 1, -1};
Fields[[10]] = {C20, 1, C2, 0, 1, 1, 1};

(*-----*)
(* Superpotential *)
(*-----*)

SuperPotential = { {{1, Yu},{u,q,Hu}}, {{-1,Yd},{d,q,Hd}},
                   {{-1,Ye},{e,l,Hd}}, {{1,[Mu]},{Hu,Hd}},
                   {{1,Yv},{l,Hu,vR}}, {{-1,MuP},{C1,C2}},
                   {{1,Yn},{vR,C1,vR}} };

(*-----*)
(* Integrate Out or Delete Particles *)
(*-----*)

IntegrateOut={};
DeleteParticles={};

(*-----*)
(* ROTATIONS *)
(*-----*)

(* ----- Different eigenstates: gauge eigenstates and eigenstates after EWSB
    ----- *)
```

```

NameOfStates={GaugeES, EWSB};

(* ----- Gauge fixing terms for Gauge eigenstates ----- *)

DEFINITION[GaugeES][GaugeFixing]=
    { {Der[VWB], -1/(2 Rxi[W])},
      {Der[VG], -1/(2 Rxi[G])} };

(*----- Rotations in gauge sector ----- *)

DEFINITION[EWSB][GaugeSector] =
    { {{VB,VWB[3],VBp},{VP,VZ,VZp},ZZ},
      {{VWB[1],VWB[2]},{VWm conj[VWm]},ZW},
      {{fWB[1],fWB[2],fWB[3]},{fWm,fWp,fW0},ZfW} };

(*----- VEVs ----- *)

DEFINITION[EWSB][VEVs]=
    {{SHd0, {vd, 1/Sqrt[2]}, {sigmad, \[ImaginaryI]/Sqrt[2]}, {phid, 1/Sqrt[2]}},
      {SHu0, {vu, 1/Sqrt[2]}, {sigmau, \[ImaginaryI]/Sqrt[2]}, {phiu, 1/Sqrt[2]}},
      {SvL, {0, 0}, {sigmaL, \[ImaginaryI]/Sqrt[2]}, {phiL, 1/Sqrt[2]}},
      {SvR, {0, 0}, {sigmaR, \[ImaginaryI]/Sqrt[2]}, {phiR, 1/Sqrt[2]}},
      {SC10, {x1, 1/Sqrt[2]}, {sigma1, \[ImaginaryI]/Sqrt[2]}, {phi1, 1/Sqrt[2]}},
      {SC20, {x2, 1/Sqrt[2]}, {sigma2, \[ImaginaryI]/Sqrt[2]}, {phi2, 1/Sqrt[2]}} };

(*----- Matter Sector ----- *)

DEFINITION[EWSB][MatterSector]=
    { {{SdL, SdR}, {Sd, ZD}},
      {{SuL, SuR}, {Su, ZU}},
      {{SeL, SeR}, {Se, ZE}},
      {{sigmaL, sigmaR}, {SvIm, ZVI}},
      {{phiL, phiR}, {SvRe, ZVR}},
      {{phid, phiu, phi1, phi2}, {hh, ZH}},
      {{sigmad, sigmau, sigma1, sigma2}, {Ah, ZA}},
      {{SHdm, conj[SHup]}, {Hpm, ZP}},
      {{fB, fW0, FHd0, FHu0, fBp, FC10, FC20}, {L0, ZN}},
      {{fWm, FHdm}, {fWp, FHup}}, {{Lm, UM}, {Lp, UP}},
      {{FvL, conj[FvR]}, {Fvm, UV}},
      {{{FeL}, {conj[FeR]}}, {{FEL, ZEL}, {FER, ZER}}},
      {{{FdL}, {conj[FdR]}}, {{FDL, ZDL}, {FDR, ZDR}}},
      {{{FuL}, {conj[FuR]}}, {{FUL, ZUL}, {FUR, ZUR}}} \
    };

(*----- Gauge Fixing after EWSB ----- *)

DEFINITION[EWSB][GaugeFixing]=
    { {Der[VP], - 1/(2 Rxi[P])},
      {Der[VWm]+\[ImaginaryI] Mass[VWm] Rxi[W] Hpm[{1}]}, - 1/(Rxi[W])},
      {Der[VZ] - Mass[VZ] Rxi[Z] Ah[{1}]}, - 1/(2 Rxi[Z])},
      {Der[VZp] - Mass[VZp] Rxi[Zp] Ah[{2}]}, - 1/(2 Rxi[Zp])},
      {Der[VG], - 1/(2 Rxi[G])} };

(*----- Phases ----- *)

```

```

DEFINITION[EWSB][Phases]=
{
    {fG, PhaseGlu}
};

(*-----*)
(*   Dirac Spinors                               *)
(*-----*)

(* Dirac Spinors for gauge eigenstates *)

DEFINITION[GaugeES][DiracSpinors]={
    Bino -> {fB, conj[fB]},
    Wino -> {fWB, conj[fWB]},
    Glu -> {fG, conj[fG]},
    H0 -> {FHd0, conj[FHu0]},
    HC -> {FHdm, conj[FHup]},
    Fd1 -> {FdL, 0},
    Fd2 -> {0, FdR},
    Fu1 -> {FuL, 0},
    Fu2 -> {0, FuR},
    Fe1 -> {FeL, 0},
    Fe2 -> {0, FeR},
    Fv1 -> {FvL, 0},
    Fv2 -> {0, FvR},
    FC -> {FC10, conj[FC20]},
    FB -> {fBp, conj[fBp]}
};

(* Dirac Spinors for eigenstates after EWSB *)

DEFINITION[EWSB][DiracSpinors]={
    Fd -> { FDL, conj[FDR]},
    Fe -> { FEL, conj[FER]},
    Fu -> { FUL, conj[FUR]},
    Fv -> { Fvm, conj[Fvm]},
    Chi -> { L0, conj[L0]},
    Cha -> { Lm, conj[Lp]},
    Glu -> { fG, conj[fG]}
};

```

C.2 SPheno.m

```

(*-----*)
(*   MINPAR                                       *)
(*-----*)

MINPAR={ {1,m0},
          {2,m12},
          {3,TanBeta},
          {4,SignumMu},
          {5,Azero},
          {6,SignumMuP},
          {7,TanBetaP},
          {8,MZp}};

RealParameters = {TanBeta, TanBetaP};

(*-----*)
(*   Tadpoles and renormalization scale          *)
(*-----*)

```

```

(*-----*)

ParametersToSolveTadpoles = {B[\[Mu]],B[MuP],\[Mu],MuP};

RenormalizationScaleFirstGuess = m0^2 + 4 m12^2;
RenormalizationScale = MSu[1]*MSu[6];

(*-----*)
(*      Boundary conditions      *)
% (*-----*)

(* ----- Definition of GUT scale ----- *)
ConditionGUTscale = (g1*g1p-g1g1p*g1pg1)/Sqrt[g1p^2+g1pg1^2] == g2;

(* ----- Boundary conditions at GUT scale ----- *)
BoundaryHighScale={
{g1,(g1*g1p-g1g1p*g1pg1)/Sqrt[g1p^2-g1pg1^2]},
{g1,Sqrt[(g1^2+g2^2)/2]},
{g2,g1},
{g1p,g1},
{g1g1p,0},
{g1pg1,0},
{T[Ye],Azero*Ye},
{T[Yd],Azero*Yd},
{T[Yu],Azero*Yu},
{T[Yv],Azero*Yv},
{T[Yn],Azero*Yn},
{mq2,DIAGONAL m0^2},
{ml2,DIAGONAL m0^2},
{md2,DIAGONAL m0^2},
{mu2,DIAGONAL m0^2},
{me2,DIAGONAL m0^2},
{mvR2,DIAGONAL m0^2},
{mHd2,m0^2},
{mHu2,m0^2},
{mC12,m0^2},
{mC22,m0^2},
{MassB,m12},
{MassWB,m12},
{MassG,m12},
{MassBp,m12},
{MassBBp,0},
{MassBpB,0}
};

(* ----- Boundary conditions at SUSY scale ----- *)
BoundarySUSYScale = {
{g1T,(g1*g1p-g1g1p*g1pg1)/Sqrt[g1p^2+g1pg1^2]},
{g1pT,Sqrt[g1p^2+g1pg1^2]},
{g1g1pT,(g1g1p*g1p+g1pg1*g1)/Sqrt[g1p^2+g1pg1^2]},
{g1,g1T},
{g1p,g1pT},
{g1g1p,g1g1pT},
{g1pg1,0},
{vevP,MZp/g1p},
{betaP,ArcTan[TanBetaP]},
{x2,vevP*Cos[betaP]},
{x1,vevP*Sin[betaP]},
{Yv,LHInput[Yv]},
{Yn,LHInput[Yn]}
}

```

```

};

(* ——— Boundary conditions at EWSB scale ——— *)
BoundaryEWSBScale = {
  {g1T, (g1*g1p-g1g1p*g1pg1)/Sqrt[g1p^2+g1pg1^2]},
  {g1pT, Sqrt[g1p^2+g1pg1^2]},
  {g1g1pT, (g1g1p*g1p+g1pg1*g1)/Sqrt[g1p^2+g1pg1^2]},
  {g1, g1T},
  {g1p, g1pT},
  {g1g1p, g1g1pT},
  {g1pg1, 0},
  {vevP, MZp/g1p},
  {betaP, ArcTan[TanBetaP]},
  {x2, vevP*Cos[betaP]},
  {x1, vevP*Sin[betaP]}
};

(* ——— Initialization values ——— *)
InitializationValues = {
  {g1p, 0.5},
  {g1g1p, -0.06},
  {g1pg1, -0.06}
}

(* ——— Boundary conditions for SUSY scale input ——— *)
BoundaryLowScaleInput={
  {vd, Sqrt[4 mz2/(g1^2+g2^2)]*Cos[ArcTan[TanBeta]]},
  {vu, Sqrt[4 mz2/(g1^2+g2^2)]*Sin[ArcTan[TanBeta]]}
};

(*—————*)
(* Two and Three body decays *)
(*—————*)

ListDecayParticles = Automatic;
ListDecayParticles3B =Automatic;

```

References

- [1] W. Emam and S. Khalil, Eur. Phys. J. C **55** (2007) 625 [arXiv:0704.1395 [hep-ph]].
- [2] L. Basso, A. Belyaev, S. Moretti and C. H. Shepherd-Themistocleous, Phys. Rev. D **80** (2009) 055030 [arXiv:0812.4313 [hep-ph]].
- [3] L. Basso, S. Moretti and G. M. Pruna, Phys. Rev. D **83** (2011) 055014 [arXiv:1011.2612 [hep-ph]].
- [4] L. Basso, S. Moretti and G. M. Pruna, Eur. Phys. J. C **71** (2011) 1724 [arXiv:1012.0167 [hep-ph]].
- [5] S. Khalil and A. Masiero, Phys. Lett. B **665** (2008) 374 [arXiv:0710.3525 [hep-ph]].
- [6] V. Barger, P. Fileviez Perez and S. Spinner, Phys. Rev. Lett. **102** (2009) 181802 [arXiv:0812.3661 [hep-ph]].

- [7] P. Fileviez Perez and S. Spinner, Phys. Rev. D **83** (2011) 035004 [arXiv:1005.4930 [hep-ph]].
- [8] J. Pelto, I. Vilja and H. Virtanen, arXiv:1012.3288 [hep-ph].
- [9] K. S. Babu, Y. Meng and Z. Tavartkiladze, Phys. Lett. B **681** (2009) 37 [arXiv:0901.1044 [hep-ph]].
- [10] M. Ambroso and B. A. Ovrut, Int. J. Mod. Phys. A **25** (2010) 2631 [arXiv:0910.1129 [hep-th]].
- [11] M. Ambroso and B. Ovrut, JHEP **0910** (2009) 011 [arXiv:0904.4509 [hep-th]].
- [12] B. Holdom, Phys. Lett. B **166**, 196 (1986).
- [13] K. S. Babu, C. F. Kolda and J. March-Russell, Phys. Rev. D **57** (1998) 6788 [arXiv:hep-ph/9710441].
- [14] F. del Aguila, G. D. Coughlan and M. Quiros, Nucl. Phys. B **307**, 633 (1988) [Erratum-ibid. B **312**, 751 (1989)].
- [15] F. del Aguila, J. A. Gonzalez and M. Quiros, Nucl. Phys. B **307**, 571 (1988).
- [16] Y. Mambrini, JCAP **1009** (2010) 022 [arXiv:1006.3318 [hep-ph]].
- [17] E. J. Chun, J. -C. Park and S. Scopel, JHEP **1102** (2011) 100 [arXiv:1011.3300 [hep-ph]].
- [18] Y. Mambrini, JCAP **1107**, 009 (2011) [arXiv:1104.4799 [hep-ph]].
- [19] S. Andreas, M. D. Goodsell and A. Ringwald, arXiv:1109.2869 [hep-ph].
- [20] E. Weihs and J. Zurita, JHEP **1202**, 041 (2012) [arXiv:1110.5909 [hep-ph]].
- [21] B. O’Leary, J.E. Camargo, W. Porod and F. Staub, in preparation.
- [22] R. Fonseca, M. Malinsky, W. Porod, F. Staub, Nucl. Phys. **B854**, 28-53 (2012). [arXiv:1107.2670 [hep-ph]].
- [23] P. H. Chankowski, S. Pokorski, J. Wagner, Eur. Phys. J. **C47** (2006) 187-205. [hep-ph/0601097].
- [24] D. Suematsu, Phys. Rev. D **59**, 055017 (1999) [arXiv:hep-ph/9808409].
- [25] F. Braam and J. Reuter, arXiv:1107.2806 [hep-ph].
- [26] D. M. Pierce, J. A. Bagger, K. T. Matchev and R. j. Zhang, Nucl. Phys. B **491** (1997) 3 [arXiv:hep-ph/9606211].
- [27] F. Staub, W. Porod, B. Herrmann, JHEP **1010**, 040 (2010). [arXiv:1007.4049 [hep-ph]].

- [28] L. Basso, S. Moretti and G. M. Pruna, Phys. Rev. D **82** (2010) 055018 [arXiv:1004.3039 [hep-ph]].
- [29] J. Alcaraz *et al.* [ALEPH Collaboration and DELPHI Collaboration and L3 Collaboration and], arXiv:hep-ex/0612034.
- [30] J. Erler, P. Langacker, S. Munir and E. Rojas, JHEP **0908**, 017 (2009) [arXiv:0906.2435 [hep-ph]].
- [31] K. Nakamura *et al.* [Particle Data Group], J. Phys. G **37** (2010) 075021.
- [32] G. Cacciapaglia, C. Csaki, G. Marandella and A. Strumia, Phys. Rev. D **74**, 033011 (2006) [hep-ph/0604111].
- [33] David Adams, talk given at Rencontres de Moriond, EW Interactions and Unified Theories, 3-10 March 2012.
- [34] F. Staub, B. O’Leary, M. Krauss and W. Porod, in preparation.
- [35] M. Hirsch, H. V. Klapdor-Kleingrothaus and S. G. Kovalenko, Phys. Lett. B **398** (1997) 311 [hep-ph/9701253].
- [36] Y. Grossman and H. E. Haber, Phys. Rev. Lett. **78** (1997) 3438 [hep-ph/9702421].
- [37] F. Staub, arXiv:0806.0538 [hep-ph].
- [38] F. Staub, arXiv:0909.2863 [hep-ph].
- [39] F. Staub, arXiv:1002.0840 [hep-ph].
- [40] S. P. Martin and M. T. Vaughn, Phys. Rev. D **50**, 2282 (1994) [Erratum-ibid. D **78**, 039903 (2008)] [arXiv:hep-ph/9311340].
- [41] W. Porod, Comput. Phys. Commun. **153** (2003) 275 [arXiv:hep-ph/0301101].
- [42] W. Porod and F. Staub, arXiv:1104.1573 [hep-ph].
- [43] S. Chatrchyan *et al.* [CMS Collaboration], arXiv:1202.1488 [hep-ex].
- [44] [ATLAS Collaboration], arXiv:1202.1408 [hep-ex].
- [45] P. Bechtle, O. Brein, S. Heinemeyer, G. Weiglein and K. E. Williams, Comput. Phys. Commun. **181** (2010) 138 [arXiv:0811.4169 [hep-ph]].
- [46] P. Bechtle, O. Brein, S. Heinemeyer, G. Weiglein and K. E. Williams, arXiv:1102.1898 [hep-ph].
- [47] H. E. Haber, M. Sher, Phys. Rev. **D35** (1987) 2206.
- [48] M. Drees, Phys. Rev. **D35** (1987) 2910-2913.

- [49] M. Cvetič, D. A. Demir, J. R. Espinosa, L. L. Everett, P. Langacker, Phys. Rev. **D56** (1997) 2861. [hep-ph/9703317].
- [50] Y. Zhang, H. An, X. d. Ji and R. N. Mohapatra, Phys. Rev. D **78**, 011302 (2008) [arXiv:0804.0268 [hep-ph]].
- [51] E. Ma, [arXiv:1108.4029 [hep-ph]].
- [52] M. Hirsch, M. Malinsky, W. Porod, L. Reichert, F. Staub, [arXiv:1110.3037 [hep-ph]].
- [53] R. Bernabei *et al.* [DAMA Collaboration], Eur. Phys. J. C **56** (2008) 333 [arXiv:0804.2741 [astro-ph]].
- [54] R. Bernabei, P. Belli, F. Cappella, R. Cerulli, C. J. Dai, A. d'Angelo, H. L. He and A. Incicchitti *et al.*, Eur. Phys. J. C **67** (2010) 39 [arXiv:1002.1028 [astro-ph.GA]].
- [55] G. Angloher, M. Bauer, I. Bavykina, A. Bento, C. Bucci, C. Ciemniak, G. Deuter and F. von Feilitzsch *et al.*, arXiv:1109.0702 [astro-ph.CO].
- [56] C. E. Aalseth *et al.* [CoGeNT Collaboration], Phys. Rev. Lett. **106** (2011) 131301 [arXiv:1002.4703 [astro-ph.CO]].
- [57] P. C. West, Phys. Lett. B **137** (1984) 371.
- [58] D. R. T. Jones and L. Mezincescu, Phys. Lett. B **138**, 293 (1984).

	BLI	BLII	BLIII	BLIV	BLV
	Bino LSP	Light Higgs	Higgsino LSP	BLino LSP	Bileptino LSP
Input					
m_0 [GeV]	1000	600	3500	3000	1000
$M_{1/2}$ [GeV]	1200	1400	1000	2500	1500
$\tan \beta$	10	20	46	40	20
$\text{sign}(\mu)$	1	1	1	1	1
A_0 [GeV]	-1000	-1000	0	1500	-1500
$\text{sign}(\mu')$	1	1	1	1	1
$\tan \beta'$	1.07	1.055	1.34	1.20	1.15
$M_{Z'}$ [GeV]	3000	2750	3600	2000	2500
$Y_{x,11}$	0.41	0.43	0.42	0.42	0.37
$Y_{x,22}$	0.41	0.43	0.42	0.42	0.40
$Y_{x,33}$	0.41	0.43	0.36	0.42	0.40
CP-even Higgs sector					
m_{h_1} [GeV]	110.1	14.7	122.9	124.1	123.9
m_{h_2} [GeV]	124.2	123.6	849.2	273.9	208.1
m_{h_3} [GeV]	1934.3	1877.3	2042.3	3008.7	2165.0
m_{h_4} [GeV]	4044.1	3414.5	5914.8	6830.5	3007.8
$ Z_{13}^H ^2 + Z_{14}^H ^2$	0.8471	0.9978	0.0002	0.0046	0.0026
$ Z_{23}^H ^2 + Z_{24}^H ^2$	0.1529	0.0022	0.9998	0.9954	0.9973
$\Gamma(h_{SM})$ [MeV]	2.22	2.47	2.43	4.15	2.47
$\text{Br}(h_{SM} \rightarrow \gamma\gamma) \cdot 10^{-3}$	4.13	4.29	4.28	2.61	4.34
Neutralino sector					
$m_{\tilde{\chi}_1^0}$ [GeV]	583.3	681.1	461.6	22.3	678.0
$m_{\tilde{\chi}_2^0}$ [GeV]	987.0	1150.9	501.8	1284.0	735.1
$m_{\tilde{\chi}_3^0}$ [GeV]	1501.0	1222.6	525.9	2025.9	1241.9
$m_{\tilde{\chi}_4^0}$ [GeV]	1508.0	1688.0	863.3	2063.0	1827.0
$m_{\tilde{\chi}_5^0}$ [GeV]	1673.3	1694.0	1783.9	2148.0	1867.5
$m_{\tilde{\chi}_6^0}$ [GeV]	1967.0	1845.4	2672.5	3876.5	1871.5
$m_{\tilde{\chi}_7^0}$ [GeV]	4139.3	3651.5	4876.2	4897.9	3131.4
$ Z_{11}^N ^2 + Z_{12}^N ^2$	0.9975	0.9975	0.4441	0.0137	$O(10^{-5})$
$ Z_{13}^N ^2 + Z_{14}^N ^2$	0.0017	0.0013	0.5558	$O(10^{-6})$	$O(10^{-7})$
$ Z_{15}^N ^2$	$O(10^{-5})$	$O(10^{-5})$	$O(10^{-5})$	0.7770	0.0032
$ Z_{16}^N ^2 + Z_{17}^N ^2$	0.0007	0.0012	0.0001	0.2092	0.9967

Table 2: Points with distinct features: BLI is similar to the MSSM with a bino LSP, BLII provides a very light, bilepton-like Higgs boson, BLIII has a very large Higgsino fraction, BLIV has a BLino LSP and sizable mixing between the doublets and bileptons in the Higgs sector, and BLV has a bileptino LSP. h_{SM} denotes the Higgs fields which is most similar to the SM Higgs particle.

particle	MSSM ^{1L}	$B - L$ ^{1L} _{NKM}	$B - L$ ^{1L} _{KM}	MSSM ^{2L}	B-L ^{2L} _{NKM}	B-L ^{2L} _{KM}
\tilde{d}_1	2280.8	2272.6	2273.2	2244.7	2234.6	2235.3
\tilde{d}_2	2429.8	2442.3	2449.9	2403.4	2414.7	2421.8
$\tilde{d}_{3,4}$	2445.5	2457.9	2465.5	2418.7	2430.0	2437.0
$\tilde{d}_{5,6}$	2570.9	2563.2	2564.2	2519.4	2509.7	2510.9
\tilde{u}_1	1832.5	1848.5	1834.0	1828.7	1842.4	1828.9
\tilde{u}_2	2301.3	2294.1	2294.2	2266.7	2257.8	2258.1
$\tilde{u}_{3,4}$	2459.3	2471.4	2461.3	2428.9	2439.1	2429.6
$\tilde{u}_{5,6}$	2569.7	2561.9	2563.0	2518.2	2508.5	2509.7
\tilde{e}_1	1087.2	1064.3	1056.3	1078.1	1043.4	1040.9
$\tilde{e}_{2,3}$	1103.1	1080.4	1072.9	1093.8	1059.4	1057.3
\tilde{e}_4	1287.6	1379.7	1356.1	1259.9	1345.3	1323.6
$\tilde{e}_{5,6}$	1293.4	1385.5	1362.1	1265.6	1351.0	1329.4
$\tilde{\nu}_{1,2,3}^R$	-	848.6	698.8	-	944.3	809.1
$\tilde{\nu}_4^R$	-	1376.7	1353.1	-	1342.2	1320.4
$\tilde{\nu}_{5,6}^R$	-	1382.9	1359.5	-	1348.3	1326.7
$\tilde{\nu}_1^{(I)}$	1284.2	1376.7	1353.1	1256.3	1342.2	1320.4
$\tilde{\nu}_{2,3}^{(I)}$	1290.6	1382.9	1359.5	1262.8	1348.3	1326.7
$\tilde{\nu}_{4,5,6}^I$	-	3321.5	3220.8	-	3307.8	3205.0
h_1	121.9	121.6	123.3	122.1	121.8	110.1
h_2	-	127.2	102.2	-	130.9	124.2
h_3	1937.0	1934.1	1920.4	1952.2	1948.3	1934.3
h_4	-	4111.0	4109.3	-	4045.4	4044.1
A^0	1937.5	1936.1	1922.3	1952.6	1950.2	1936.2
A_η^0	-	2829.0	2820.3	-	2733.9	2725.5
H^+	1941.0	1938.2	1924.4	1956.1	1952.3	1938.3
\tilde{g}	2669.9	2670.2	2670.2	2602.1	2600.9	2600.7
$\nu_{4,5,6}$	-	1046.9	1046.5	-	987.6	987.2
$\tilde{\chi}_1^+$	1046.3	1477.5	1467.4	988.5	1518.4	1508.2
$\tilde{\chi}_2^+$	1480.7	3023.5	3020.4	1522.6	3023.2	3020.1
$\tilde{\chi}_1^0$	550.3	550.3	598.4	534.8	533.9	583.3
$\tilde{\chi}_2^0$	1046.2	1046.8	1046.3	988.3	987.4	987.0
$\tilde{\chi}_3^0$	1472.2	1468.9	1458.4	1515.7	1511.6	1501.0
$\tilde{\chi}_4^0$	1480.5	1477.3	1467.3	1522.3	1518.2	1508.0
$\tilde{\chi}_5^0$	-	1749.0	1729.0	-	1695.2	1673.3
$\tilde{\chi}_6^0$	-	1959.6	1947.5	-	1978.0	1966.9
$\tilde{\chi}_7^0$	-	4175.5	4183.5	-	4131.2	4139.3

Table 3: Comparison of mass spectrum in the MSSM and the BLSSM for input parameters BLI of Tab. 2. We give the masses for one- and two-loop RGE-evaluations. In addition, we include a comparison of the case of properly taking into account gauge kinetic mixing (KM) versus neglecting it (NKM).